Modeling dual drug delivery from eluting stents: the influence of non-linear binding competition and non-uniform drug loading

Swapnil Salvi[1], Ankur Jain[1], Giuseppe Pontrelli[2], Sean McGinty[3,4]

1 - Mechanical and Aerospace Engineering Department, University of Texas at Arlington, Arlington, TX, USA

2 - Istituto per le Applicazioni del Calcolo – CNR Via dei Taurini 19, Rome 00185, Italy

3 - Division of Biomedical Engineering, University of Glasgow, Glasgow, UK

4 - Glasgow Computational Engineering Centre, University of Glasgow, Glasgow, UK

[*] – Corresponding Author: email: jaina@uta.edu; Ph: +1 (817) 272-9338
500 W First St, Rm 211, Arlington, TX, USA 76019

CRediT Authorship Contribution Statement

S. Salvi –Methodology, Formal Analysis, Validation, Investigation, Data Curation; A. Jain – Conceptualization, Methodology, Formal Analysis, Validation, Investigation, Data Curation, Supervision, Project Administration; G. Pontrelli – Conceptualization, Methodology, Formal Analysis, Validation; S. McGinty – Conceptualization, Methodology, Formal Analysis, Validation. All authors contributed towards Writing Original Draft, Review and Editing.

Abstract

Objective: There is increasing interest in simultaneous endovascular delivery of more than one drug from a drug-loaded stent into a diseased artery. There may be an opportunity to obtain a therapeutically desirable uptake profile of the two drugs over time by appropriate design of the initial drug distribution in the stent. Due to the non-linear, coupled nature of diffusion and reversible specific/non-specific binding of both drugs as well as competition between the drugs for a fixed binding site density, a comprehensive numerical investigation of this problem is critically needed.

Methods: This paper presents numerical computation of dual-drug delivery in a stent-artery system, accounting for diffusion as well as specific and non-specific reversible binding. The governing differential equations are discretized in space, followed by integration over time using a stiff numerical solver. Three different cases of initial dual drug distribution are considered.

Results: For the particular case of sirolimus and paclitaxel, results show that competition for a limited non-specific binding site density, and the significant difference in the forward/backward reaction coefficients plays a key role in determining the nature of drug uptake. The nature of initial distribution of the two drugs in the stent is also found to influence the binding process, which can potentially be used to engineer a desirable dual drug uptake profile.

Conclusions: These results help improve the fundamental understanding of endovascular dual drug delivery. In addition, the numerical technique and results presented here may be helpful for designing and optimizing other drug delivery problems as well.

Keywords: Endovascular Drug Delivery; Stent; Dual-Drug Delivery; Specific Binding; Non-Specific Binding; Numerical Computation.

Nomenclature

b	bound drug concentration ($mol \cdot m^{-3}$)
B	binding site density ($mol \cdot m^{-3}$)
c	free drug concentration ($mol \cdot m^{-3}$)
D	diffusion coefficient ($m^2 \cdot s^{-1}$)
h	convective mass transfer coefficient ($m \cdot s^{-1}$)
Sh	Sherwood number
t	time (s)
x	spatial coordinate (m)
γ	non-dimensional interface location
μ	forward reaction coefficient for binding $(mol \cdot m^{-3} \cdot s)^{-1}$
σ	reverse reaction coefficient for binding (s^{-1})
τ	non-dimensional time
ψ	non-dimensional amount of bound drug remaining
χ	non-dimensional amount of drug lost
ρ	non-dimensional amount of free drug remaining
ξ	non-dimensional spatial coordinate

Subscripts

m	layer number
ref	reference value
in	initial value

Superscripts

A,B	drugs A and B
ns	non-specific binding
s	specific binding

Overbars refer to non-dimensional quantities

1. Introduction

Mathematical and computational modeling of drug delivery devices has been gaining in momentum over the past two decades. Such models typically aim to better understand the mechanisms of drug release and/or subsequent drug transport and retention within the biological environment. The *piece de resistance* is the use of the model to infer the optimal design parameters (e.g. drug physicochemical properties, drug dose, drug release rate and loading strategy) to achieve the desired biological effect. In this quest, models have been increasing in sophistication, moving from simple descriptions of drug release from the device in simple *in vitro* environments [1,2,3] to more complex models which incorporate important features of the *in vivo* environment [4,5,6].

Drug-Eluting Stents (DESs) for the treatment of obstructive coronary artery disease are a class of drug delivery device that has received significant attention in the modeling literature [7]. Over the past two decades, modeling has played an important role in explaining deficiencies with early devices, and has helped inform subsequent generations of stents. For example, through modeling, the importance of drug lipophilicity was uncovered, explaining why heparin-coated stents underperform when compared to paclitaxel- and sirolimus-coated stents [8]. Moreover, particularly in the case of sirolimus-eluting stents, modeling has revealed that it is more important to tune drug-elution rate to sustain saturation of specific-binding sites within tissue than to ramp up the drug dose [4,9]. Accounting for the different physicochemical properties of paclitaxel and sirolimus, computational modeling has revealed different 'optimal' drug release strategies for these two drugs [5]. Furthermore, modeling has uncovered the importance of accounting for both specific and non-specific binding within arterial tissue [6]. While the state-of-the-art computational models in this field are 2D-axisymmetric and multilayer, incorporating anisotropic

diffusion properties, layer-specific parameters and two phases of nonlinear saturable binding [2], many of the aforementioned discoveries have been made based upon simpler one-dimensional models [4,6,8,9].

To the best of our knowledge, the existing DES modeling literature considers the delivery of only a single drug, reflecting the current clinical state-of-the-art. However, the idea of dual DES (D-DES) (i.e. stents coated with two different drugs) was conceived several years ago and there have been a number of studies in the literature investigating different combinations of drugs [10]. Initially, it was hypothesized that paclitaxel and sirolimus could be delivered from a D-DES to reap the benefits of both drugs, following the success of early paclitaxel DESs and sirolimus DESs [10]. Each of these drugs targets smooth muscle cell proliferation, albeit via different mechanisms. Several subsequent studies have attempted to combine alternative drugs (e.g. sirolimus and heparin/probucol/genistein/triflusal, zotarolimus and dexamethasone, paclitaxel and pimecrolimus/cilostazol, atorvastatin and fenofibrate) that target different combinations of complications associated with DES placement, for example restenosis, thrombosis and delayed endothelial healing [11-15].

As well as the clinical relevance, the simultaneous or staggered delivery of two different drugs with different physicochemical properties is interesting both from a computational modeling and an optimization point of view. The state-of-the-art models of drug delivery to arterial tissue assume two independent phases of nonlinear reversible drug binding: on one hand, drug binds specifically to target receptors within cells, while on the other hand, drugs may bind to non-specific binding sites within the extracellular matrix (Figure 1(a)). Each binding phase contributes to drug retention, while specific binding is thought to be most important in terms of efficacy [9]. While

specific binding is drug-dependent, it is probable that different drugs will compete for non-specific binding sites: this introduces coupling, meaning that it is not possible to solve two independent drug-delivery problems. Depending on the drug release strategy, this has the potential to lead to saturation of non-specific binding sites, with a subsequent impact on total content of each drug within tissue. Moreover, drug binding may, in general, be reversible or non-reversible (Figure 1(a)). Different binding on and off rates between different drugs is likely to alter the time course of drug availability for binding to specific receptors. It then follows that the initial loading configuration of each drug on the D-DES will have an impact on the binding dynamics and drug retention within the tissue. This introduces the possibility of engineering the initial distribution of the two drugs on the D-DES to achieve a desired time course of drug-uptake and binding within the tissue. Practical considerations to be modeled and optimized include the spatial distribution of the two drugs in the stent – for example, should both drug be distributed uniformly, or should one drug be distributed closer to the artery-side of the stent, in order to promote early binding of that drug. Comprehensive modeling of drug diffusion, reversible binding – both specific and non-specific – and convective loss is needed in order to answer such questions.

This paper presents a theoretical model of D-DES delivery and retention within tissue, accounting for both reversible specific binding as well as reversible non-specific binding, in which both drugs compete for a finite binding site density. Building upon past work [1], the three novel features of the present work from a modeling point of view are (i) the delivery of two different drugs; (ii) the introduction of a competitive nonlinear saturable binding mechanism; and (iii) the consideration of different spatial drug loading configurations. The inherent nonlinearity in the problem prohibits the development of an exact solution, and therefore, we develop a robust numerical method based on finite difference technique to solve the underlying coupled reversible

two-layer nonlinear diffusion-reaction equations. We utilise the model to simulate spatio-temporal drug concentrations within the D-DES and tissue and examine important indices such as drug content in tissue, specific and non-specific bound drug, as a fraction of the total available binding sites.

2. Problem Definition

Consider the simultaneous delivery of two drugs, A and B, from a stent into an artery. The two-layer geometry considered here is shown in Figure 1(b), where layers 1 and 2 refer to stent coating and artery, respectively. The problem is modeled as one-dimensional, as is common in the stent modeling literature [3,9]. While the artery is, in general, a multilayer structure, it is modeled here as a homogeneous body, as has commonly been done in the literature [4,9]. This is justified on the basis of the media layer being much thicker than other layers, as well as the binding reactions primarily occurring in the media layer, where the target smooth muscle cells reside. Moreover, due to the large diameter of the artery relative to its thickness, a Cartesian coordinate system is used here. The stent coating and artery thicknesses are x_1 and $(x_2 - x_1)$, respectively, for the total domain size of x_2. Note that while the problem is presented here in the context of a stent-artery system, the model presented here, with appropriate adaptations is applicable for other drug delivery problems as well.

In general, the two drugs A and B are initially loaded with a known concentration distribution given by $c^A_{m,in}(x)$ and $c^B_{m,in}(x)$, respectively (m=1,2), and the interest is in understanding the nature of drug uptake through binding in the artery over time. Concentrations of free and bound drug A in the m^{th} layer are denoted by c^A_m and b^A_m (m=1,2), respectively, and a

similar nomenclature is followed for drug B. Starting at t=0, we assume that drugs A and B both begin to diffuse with independent, constant and uniform effective diffusion coefficients given by D_m^A and D_m^B, respectively, in the two layers m=1,2. While accounting for binding reactions within the tissue is essential, in the interest of generality, the model also allows for the possibility of drug binding/absorption within the stent coating, a phenomenon which may explain incomplete and/or delayed release of drug from certain stent platforms [2]. Binding of drugs A and B are modeled in a general and coupled fashion, accounting for reversible drug binding of both specific and non-specific type in each layer. In the latter case, within the tissue, the two drugs compete with each other for a finite density of available binding sites. The binding site density for specific binding of drug A in each layer is denoted by $B_m^{A,s}$, whereas the binding site density for non-specific binding in each layer is denoted by B_m^{ns}. Forward and reverse reaction coefficients for the specific binding process for drug A are denoted by $\mu_m^{A,s}$ and $\sigma_m^{A,s}$, respectively, for each layer m=1,2. Forward and reverse reaction coefficients for the non-specific binding process for drug A are denoted by $\mu_m^{A,ns}$ and $\sigma_m^{A,ns}$, respectively, for each layer m=1,2. Similar nomenclature is followed for drug B. Note that in some cases, there may be no binding in the stent coating layer, for which, the corresponding coefficients may be set to zero. Further, the general framework described above may be simplified to the case of irreversible binding by setting the reverse reaction coefficients to zero.

Based on the nomenclature and assumptions listed here, the governing equations for drug concentrations may be written as

$$\frac{\partial c_m^A}{\partial t} = \frac{\partial}{\partial x}\left(D_m^A \frac{\partial c_m^A}{\partial x}\right) - \mu_m^{A,s}\left(B_m^{A,s} - b_m^{A,s}\right)c_m^A + \sigma_m^{A,s} b_m^{A,s} - \mu_m^{A,ns}\left(B_m^{ns} - b_m^{total,ns}\right)c_m^A + \sigma_m^{A,ns} b_m^{A,ns} \qquad x_{m-1} < x < x_m \quad (m=1,2) \qquad (1)$$

$$\frac{\partial b_m^{A,s}}{\partial t} = \mu_m^{A,s}\left(B_m^{A,s} - b_m^{A,s}\right)c_m^A - \sigma_m^{A,s} b_m^{A,s} \qquad x_{m-1} < x < x_m \quad (m=1,2) \qquad (2)$$

$$\frac{\partial b_m^{A,ns}}{\partial t} = \mu_m^{A,ns}\left(B_m^{ns} - b_m^{total,ns}\right)c_m^A - \sigma_m^{A,ns} b_m^{A,ns} \qquad x_{m-1} < x < x_m \quad (m=1,2) \qquad (3)$$

Here, $b_m^{total,ns} = b_m^{A,ns} + b_m^{B,ns}$ is the total non-specific bound concentration for drugs A and B. B_m^{ns} and $B_m^{A,s}$ are the total binding site densities available for non-specific binding and for specific binding of drug A, respectively. A set of equations similar to equations (1)-(3) may also be written for drug B.

Several difficulties are likely to be encountered in solving these governing equations. Firstly, the governing equations for drugs A and B are coupled to each other through the $\left(B_m^{ns} - b_m^{total,ns}\right)$ term that appears in the equations for both drugs. This term represents competitive binding between the two drugs on a finite available binding site density. Further, the governing equations are, in general, non-linear. Approximate linearization may only carried out if the specific and non-specific bound drug concentrations are expected to be very small compared to the density of the corresponding available binding sites.

Boundary conditions associated with equations (1)-(3) (and the similar set of equations for drug B) may be written as follows:

$$\frac{\partial c_1^A}{\partial x} = \frac{\partial c_1^B}{\partial x} = 0 \qquad at\ x = 0 \text{ (4)}$$

$$-D_2^A \frac{\partial c_2^A}{\partial x} = h^A c_2^A;\ -D_2^B \frac{\partial c_2^B}{\partial x} = h^B c_2^B \qquad at\ x = x_2 \text{ (5)}$$

These equations model a non-penetrable wall at the stent/coating interface and convective mass loss to the surrounding medium at the external boundary of the arterial wall. The former is justified in practical scenarios where, for example, the drug-carrying polymer layer in a stent is backed by a metal support, which the drug cannot diffuse into. However, we note that these equations are unable to account for drug lost to the lumen. This may be regarded as the extreme case where 100% drug delivery efficiency is achieved. Extending the model to higher spatial dimensions, which is left for future work, would more readily enable the incorporation of the effects of drug lost to the lumen (see, for example, [16] and [17]). The convective boundary condition is general enough to span the entire convective spectrum between an impenetrable wall (zero convective mass transfer coefficients) and an infinite sink (very large convective mass transfer coefficients).

In addition, the following equations are assumed at the interface between the two layers:

$$c_1^A = c_2^A;\ c_1^B = c_2^B \qquad \text{at } x = x_1 \text{ (6)}$$

$$-D_1^A \frac{\partial c_1^A}{\partial x} = -D_2^A \frac{\partial c_2^A}{\partial x};\ -D_1^B \frac{\partial c_1^B}{\partial x} = -D_2^B \frac{\partial c_2^B}{\partial x} \qquad \text{at } x = x_1 \text{ (7)}$$

Equations (6) and (7) represent continuity and conservation of mass flux, respectively, at the interface.

Initial conditions associated with the problem may be written as

$$c_m^A = c_{m,in}^A(x); c_m^B = c_{m,in}^B(x) \qquad (m=1,2) \quad at\ t = 0 \ (8)$$

Equation (8) accounts for any arbitrary initial distribution of the two drugs. For example, as shown in Figure 1(b), the two drugs may be distributed uniformly, or one of the drugs may be distributed closer to the stent-artery interface, or, in general, the drug distribution may be completely arbitrary, perhaps based on patient-specific needs. In addition, it is assumedthat there is no bound drug in either layer at the initial time.

2.2. Non-dimensionalization

Due to the large number of variables and parameters involved in the problem definition outlined above, it is helpful to non-dimensionalize. For each layer, m=1,2, variables associated with drug A are non-dimensionalized as follows:

$$\bar{c}_m^A = \frac{c_m^A}{c_{ref}},\ \bar{b}_m^{A,s} = \frac{b_m^{A,s}}{c_{ref}},\ \bar{b}_m^{A,ns} = \frac{b_m^{A,ns}}{c_{ref}};\ \bar{B}_m^{A,s} = \frac{B_m^{A,s}}{c_{ref}};\ \bar{D}_m^A = \frac{D_m^A}{D_{ref}};\ \bar{\mu}_m^{A,s} = \frac{\mu_m^{A,s} c_{ref} x_2^2}{D_{ref}};\ \bar{\sigma}_m^{A,s} = \frac{\sigma_m^{A,s} x_2^2}{D_{ref}};$$

$$\bar{\mu}_m^{A,ns} = \frac{\mu_m^{A,ns} c_{ref} x_2^2}{D_{ref}}; \bar{\sigma}_m^{A,ns} = \frac{\sigma_m^{A,ns} x_2^2}{D_{ref}}; \bar{c}_{m,in}^A = \frac{c_{m,in}^A}{c_{ref}}; Sh_A = \frac{h^A x_2}{D_{ref}}; \bar{B}_m^{ns} = \frac{B_m^{ns}}{c_{ref}} \qquad (9)$$

with similar nomenclature for drug B. Note that Sh_A and Sh_B are the Sherwood numbers that characterize the nature of boundary condition at $\xi = 1$ for drugs A and B, respectively. In addition,

$$\xi = \frac{x}{x_2}, \tau = \frac{D_{ref} t}{x_2^2}, \gamma_1 = \frac{x_1}{x_2} \qquad (10)$$

Here, D_{ref} is a reference diffusion coefficient, which may be taken to be equal to one of the diffusion coefficients appearing in this problem, say, that of drug A in layer 2, D_2^A. c_{ref} is a reference drug concentration that may be obtained from the given initial drug distributions. For example, if $c_{1,in}^A(\xi)$ is constant, then one may choose $c_{ref} = c_{1,in}^A$.

Based on equations (9) and (10), the following set of non-dimensional partial differential equations for the concentrations of drug A may be written:

$$\frac{\partial \bar{c}_m^A}{\partial \tau} = \frac{\partial}{\partial \xi}\left(\bar{D}_m^A \frac{\partial \bar{c}_m^A}{\partial \xi}\right) - \bar{\mu}_m^{A,s}\left(\bar{B}_m^{A,s} - \bar{b}_m^{A,s}\right)\bar{c}_m^A + \bar{\sigma}_m^{A,s}\bar{b}_m^{A,s} - \bar{\mu}_m^{A,ns}\left(\bar{B}_m^{ns} - \bar{b}_m^{total,ns}\right)\bar{c}_m^A + \bar{\sigma}_m^{A,ns}\bar{b}_m^{A,ns} \qquad \gamma_{m-1} < \xi < \gamma_m \ (m=1,2) \qquad (11)$$

$$\frac{\partial \bar{b}_m^{A,s}}{\partial \tau} = \bar{\mu}_m^{A,s}\left(\bar{B}_m^{A,s} - \bar{b}_m^{A,s}\right)\bar{c}_m^A - \bar{\sigma}_m^{A,s}\bar{b}_m^{A,s} \qquad \gamma_{m-1} < \xi < \gamma_m \ (m=1,2) \qquad (12)$$

$$\frac{\partial \bar{b}_m^{A,ns}}{\partial \tau} = \bar{\mu}_m^{A,ns}\left(\bar{B}_m^{ns} - \bar{b}_m^{total,ns}\right)\bar{c}_m^A - \bar{\sigma}_m^{A,ns}\bar{b}_m^{A,ns} \qquad \gamma_{m-1} < \xi < \gamma_m \ (m=1,2) \qquad (13)$$

with a similar set of equations for drug B. Note that $\bar{b}_m^{total,ns} = \bar{b}_m^{A,ns} + \bar{b}_m^{B,ns}$. Further, in equations (11)-(13), the nomenclature $\gamma_0 = 0$ and $\gamma_2 = 1$ is used.

The following boundary and interface conditions may be written:

$$\frac{\partial \bar{c}_1^A}{\partial \xi} = \frac{\partial \bar{c}_1^B}{\partial \xi} = 0 \qquad at\ \xi = 0 \ (14)$$

$$-\bar{D}_2^A \frac{\partial \bar{c}_2^A}{\partial \xi} = Sh_A \bar{c}_2^A;\ -\bar{D}_2^B \frac{\partial \bar{c}_2^B}{\partial \xi} = Sh_B \bar{c}_2^B \qquad at\ \xi = 1 \quad (15)$$

$$\bar{c}_1^A = \bar{c}_2^A;\ \bar{c}_1^B = \bar{c}_2^B \qquad \text{at } \xi = \gamma_1 \quad (16)$$

$$-\bar{D}_1^A \frac{\partial \bar{c}_1^A}{\partial \xi} = -\frac{\partial \bar{c}_2^A}{\partial \xi};\ -\bar{D}_1^B \frac{\partial \bar{c}_1^B}{\partial \xi} = -\frac{\partial \bar{c}_2^B}{\partial \xi} \qquad \text{at } \xi = \gamma_1 \quad (17)$$

The initial conditions are

$$\bar{c}_m^A = \bar{c}_{m,in}^A(\xi);\ \bar{c}_m^B = \bar{c}_{m,in}^B(\xi) \qquad (m\text{=}1,2) \quad \text{at } \tau = 0 \quad (18)$$

This completes the problem definition in non-dimensional form. It is of interest to solve these equations in order to understand the nature of dual-drug binding, specifically, the competition between drugs A and B for non-specific binding sites, and the interaction between diffusion and binding processes. The effect of the initial loading of the drugs, i.e., $\bar{c}_{m,in}^A(\xi)$ and $\bar{c}_{m,in}^B(\xi)$ on drug uptake is also of particular interest.

These equations, in general, contain twelve drug concentration distributions – $\bar{c}_1^A$, $\bar{b}_1^{A,s}$, $\bar{b}_1^{A,ns}$, $\bar{c}_2^A$, $\bar{b}_2^{A,s}$, $\bar{b}_2^{A,ns}$, $\bar{c}_1^B$, $\bar{b}_1^{B,s}$, $\bar{b}_1^{B,ns}$, $\bar{c}_2^B$, $\bar{b}_2^{B,s}$, $\bar{b}_2^{B,ns}$. These include free, non-specifically bound and specifically bound drug concentrations for drugs A and B in layers 1 and 2. However, for particular special cases, the number of variables may be lower. For example, in the case of drug delivery from a stent into an artery, it may be reasonable to neglect drug binding within the stent itself, in which case, the forward and reverse binding reaction coefficients for layer 1 are zero, and diffusion is the only relevant transport process in the stent layer. Therefore, the drug concentrations distributions of relevance for this problem are $\bar{c}_1^A$, $\bar{c}_2^A$, $\bar{b}_2^{A,s}$, $\bar{b}_2^{A,ns}$, $\bar{c}_1^B$, $\bar{c}_2^B$, $\bar{b}_2^{B,s}$ and $\bar{b}_2^{B,ns}$.

Due to the considerable complexity of these equations, an exact solution is not likely possible, except under special cases. These special cases pertain to irreversible drug binding, modeled by setting the reverse reaction coefficients $\bar{\sigma}$ to zero and linearizing the forward reaction terms by assuming the concentration of bound drug to be small. By doing so, this reduces to a two-layer problem with diffusion and irreversible consumption, for which, an exact solution is derivable using the method of separation of variables. An even more extreme scenario may be arrived at by setting all reaction coefficients $\bar{\mu}$ and $\bar{\sigma}$ to zero, which eliminates binding completely, thus reducing this to a two-layer pure-diffusion problem, for which an exact solution is also similarly derivable. For the general case considered here, however, only a numerical solution is likely to be possible. Equations (11)-(18) are solved numerically, as described in the next section.

3. Numerical Solution

Equations (11)-(18) are discretized spatially over a grid of uniform spacing in each layer, followed by integration over time using a stiff numerical solver. A total of N_1 and N_2 grid points are placed in layers 1 and 2, so that the grid spacing in each layer is given by $\Delta\xi_1 = \frac{\gamma_1}{N_1-1}$ and $\Delta\xi_2 = \frac{1-\gamma_1}{N_2-1}$. The j^{th} node in layer 1 is located at $\xi = (j-1)\Delta\xi_1$ (j=1,2,…,N_1) and the j^{th} node is layer 2 is located at $\xi = \gamma_1 + (j-1)\Delta\xi_2$ (j=1,2,...,N_2). Note that in this scheme, one node is located at the interface between the two layers and is shared between the two. In order to carry out numerical integration over time, the following expressions are derived for the time derivatives for concentrations at each node using central differencing:

For all internal nodes,

$$\frac{\partial \bar{c}_m^A(j)}{\partial \tau} = \bar{D}_m^A \frac{\bar{c}_m^A(j-1) + \bar{c}_m^A(j+1) - 2\bar{c}_m^A(j)}{\Delta \xi_m^2}$$
$$- \bar{\mu}_m^{A,s} \left(\bar{B}_m^{A,s} - \bar{b}_m^{A,s}(j) \right) \bar{c}_m^A(j) + \bar{\sigma}_m^{A,s} \bar{b}_m^{A,s}(j) \qquad (m=1,2) \qquad (19)$$
$$- \bar{\mu}_m^{A,ns} \left(\bar{B}_m^{ns} - \bar{b}_m^{AB,ns}(j) \right) \bar{c}_m^A(j) + \bar{\sigma}_m^{A,ns} \bar{b}_m^{A,ns}(j)$$

$$\frac{\partial \bar{b}_m^{A,s}(j)}{\partial \tau} = \bar{\mu}_m^{A,s} \left(\bar{B}_m^{A,s} - \bar{b}_m^{A,s}(j) \right) \bar{c}_m^A(j) - \bar{\sigma}_m^{A,s} \bar{b}_m^{A,s}(j) \qquad (m=1,2) \qquad (20)$$

$$\frac{\partial \bar{b}_m^{A,ns}(j)}{\partial \tau} = \bar{\mu}_m^{A,ns} \left(\bar{B}_m^{ns} - \bar{b}_m^{AB,ns}(j) \right) \bar{c}_m^A(j) - \bar{\sigma}_m^{A,ns} \bar{b}_m^{A,ns}(\mathrm{j}) \qquad (m=1,2) \qquad (21)$$

where $\bar{c}_m^A(j)$ denotes the discretized value of $\bar{c}_m^A$ at the j^{th} node, and so forth. Equations (19)-(21) are written for j=2,...,N_1-1 for the stent, and j=2,…,N_2-1 for the artery.

Note that equations for the boundary and interface nodes need to be written separately, since straightforward central differencing is not possible at these nodes, and equations for these nodes must also account for boundary/interface conditions.

For the left boundary, central differencing using a ghost node may be combined with the impermeable boundary condition, equation (14) to write

$$\frac{\partial \bar{c}_1^A(1)}{\partial \tau} = 2\bar{D}_m^A \frac{\bar{c}_1^A(2) - 2\bar{c}_1^A(1)}{\Delta \xi_1^2} \qquad (m=1,2) \qquad (22)$$

For the right boundary, one may similarly combine central differencing using a ghost node with the convective mass transfer boundary condition, equation (15) to write

$$\frac{\partial \bar{c}_2^A(N_2)}{\partial \tau} = 2\bar{D}_2^A \frac{\bar{c}_2^A(N_2-1) - 2\left(1+\Delta\xi_2 \frac{Sh_A}{\bar{D}_2^A}\right)\bar{c}_2^A(N_2)}{\Delta\xi_2^2} \qquad (m=1,2) \qquad (23)$$

The treatment of the interface node is somewhat more involved. Following the previously proposed procedure of interface node in a multilayer problem [18], the following equations are written based on backward and forward finite differencing in two nodes adjacent to the interface node in each layer:

$$\bar{c}_1^A(N_1-1) = \bar{c}_1^A(N_1) - \Delta\xi_1 \frac{\partial \bar{c}_1^A}{\partial \xi} + \frac{\Delta\xi_1^2}{2}\frac{\partial^2 \bar{c}_1^A}{\partial \xi^2} \qquad (24)$$

$$\bar{c}_1^A(N_1-2) = \bar{c}_1^A(N_1) - 2\Delta\xi_1 \frac{\partial \bar{c}_1^A}{\partial \xi} + 2\Delta\xi_1^2 \frac{\partial^2 \bar{c}_1^A}{\partial \xi^2} \qquad (25)$$

$$\bar{c}_2^A(2) = \bar{c}_2^A(1) + \Delta\xi_2 \frac{\partial \bar{c}_2^A}{\partial \xi} + \frac{\Delta\xi_2^2}{2}\frac{\partial^2 \bar{c}_2^A}{\partial \xi^2} \qquad (26)$$

$$\bar{c}_2^A(3) = \bar{c}_2^A(1) + 2\Delta\xi_2 \frac{\partial \bar{c}_2^A}{\partial \xi} + 2\Delta\xi_2^2 \frac{\partial^2 \bar{c}_2^A}{\partial \xi^2} \qquad (27)$$

where the derivatives refer to values at the interface, evaluated in the respective layer.

In addition, based on interface conditions, one may also write

$$\bar{c}_1^A(N_1) = \bar{c}_2^A(1) \qquad (28)$$

$$\bar{D}_1^A \frac{\partial \bar{c}_1^A}{\partial \xi} = \bar{D}_2^A \frac{\partial \bar{c}_2^A}{\partial \xi} \qquad (29)$$

Note that all derivatives in equations (24)-(29) are evaluated at the interface node. Equations (24)-(29) represent six linear algebraic equations in six unknowns – $\bar{c}_1^A(N_1)$, $\bar{c}_2^A(1)$, $\frac{\partial \bar{c}_1^A}{\partial \xi}$,

$\frac{\partial \bar{c}_2^A}{\partial \xi}$, $\frac{\partial^2 \bar{c}_1^A}{\partial \xi^2}$ and $\frac{\partial^2 \bar{c}_2^A}{\partial \xi^2}$. A solution for these equations is somewhat cumbersome but nevertheless derivable. In particular, expressions for the second derivatives are of interest because the diffusion term at the interface may be written approximately as the mean of $\frac{\partial^2 \bar{c}_1^A}{\partial \xi^2}$ and $\frac{\partial^2 \bar{c}_2^A}{\partial \xi^2}$ in the two layers. Based on the expressions for these terms resulting from the treatment above, the following expression for the time derivative of concentration at the interface node may be derived:

$$\frac{\partial \bar{c}_1^A(N_1)}{\partial \tau} = \bar{D}_2^A \frac{[4\bar{D}_1^A \Delta\xi_2 \bar{c}_1^A(N_1-1) - \bar{D}_1^A \Delta\xi_2 \bar{c}_1^A(N_1-2) - 6\bar{D}_1^A \Delta\xi_2 \bar{c}_2^A(2) + 3\bar{D}_1^A \Delta\xi_2 \bar{c}_2^A(3) - 2\bar{D}_2^A \Delta\xi_1 \bar{c}_2^A(2) + 2\bar{D}_2^A \Delta\xi_1 \bar{c}_2^A(3)]}{6\Delta\xi_2^2(\bar{D}_1^A \Delta\xi_2 + \bar{D}_2^A \Delta\xi_1)}$$

$$-\bar{D}_1^A \frac{[2\bar{D}_1^A \Delta\xi_2 \bar{c}_1^A(N_1-1) + 6\bar{D}_2^A \Delta\xi_1 \bar{c}_1^A(N_1-1) - 2\bar{D}_1^A \Delta\xi_2 \bar{c}_1^A(N_1-2) - 3\bar{D}_2^A \Delta\xi_1 \bar{c}_2^A(N_1-2) - 4\bar{D}_2^A \Delta\xi_1 \bar{c}_2^A(2) + \bar{D}_2^A \Delta\xi_1 \bar{c}_2^A(3)]}{6\Delta\xi_1^2(\bar{D}_1^A \Delta\xi_2 + \bar{D}_2^A \Delta\xi_1)} \quad (30)$$

Equations (19)-(23) and (30) together define a set of ordinary differential equations in concentrations at the discretized nodes, which can be numerically integrated over time. Similar equations may be written for drug B as well. Note the coupling between the equations for drugs A and B through the $\bar{b}_m^{total,ns}$ term that represents competition between drugs A and B for non-specific binding sites. Depending on the values of the parameters, the discretized equations may present difficulties in numerical computation. For example, it is common for the thickness of the drug-carrying stent layer to be much smaller than the thickness of the artery, in which case, a stiff numerical solver may be needed to reconcile the significant variation in length scale. In the present work, this integration is carried out using a stiff ODE solver that utilizes a modified Rosenbrock formula of the second order [19].

4. Overall drug delivery indicators

Several integral quantities may be defined to characterize the nature of diffusion and binding processes. The total amount of free drug A remaining in layers 1 and 2 at any time may be written in non-dimensional normalized form as follows:

$$\bar{\rho}_m^A(\tau) = \frac{1}{\gamma_1} \int_{\gamma_{m-1}}^{\gamma_m} \bar{c}_m^A(\xi^*, \tau) d\xi^* \qquad (m=1,2) \qquad (31)$$

where the normalization is carried out on the basis of the reference concentration c_{ref} and the thickness of the drug-carrying layer 1.

Similarly, the total normalized amount of drug A bound in specific and non-specific forms may be written as

$$\bar{\psi}_m^{A,s}(\tau) = \frac{1}{\gamma_1} \int_{\gamma_{m-1}}^{\gamma_m} \bar{b}_m^{A,s}(\xi^*, \tau) d\xi^*; \; \bar{\psi}_m^{A,ns}(\tau) = \frac{1}{\gamma_1} \int_{\gamma_{m-1}}^{\gamma_m} \bar{b}_m^{A,ns}(\xi^*, \tau) d\xi^* \qquad (m=1,2) \qquad (32)$$

Finally, the total amount of drug A lost at the right boundary up to a given time may be written as

$$\bar{\chi}_2^A(\tau) = \frac{Sh}{\gamma_1} \int_0^{\tau} \bar{c}_2^A(1, \tau^*) d\tau^* \qquad (33)$$

Equations similar to the ones above may also be written for drug B.

Clearly, for overall mass conservation at any time, one must have

$$\bar{\rho}_1^A(\tau) + \bar{\rho}_2^A(\tau) + \bar{\psi}_1^{A,s}(\tau) + \bar{\psi}_2^{A,s}(\tau) + \bar{\psi}_1^{A,ns}(\tau) + \bar{\psi}_2^{A,ns}(\tau) + \bar{\chi}_2^A(\tau)$$
$$= \frac{1}{\gamma_1}\int_0^{\gamma_1} \bar{c}_{1,in}^A(\xi^*,\tau)d\xi^* + \frac{1}{\gamma_1}\int_{\gamma_1}^1 \bar{c}_{2,in}^A(\xi^*,\tau)d\xi^* \quad (34)$$

and similarly for drug B.

Several terms defined above reduce to zero for common scenarios. For example, no binding reactions commonly occur in the drug-carrying stent layer (layer 1) of a stent-artery system. In this specific scenario, when the drug is uniformly loaded in the stent, the overall mass conservation simplifies to

$$\bar{\rho}_1^A(\tau) + \bar{\rho}_2^A(\tau) + \bar{\psi}_2^{A,s}(\tau) + \bar{\psi}_2^{A,ns}(\tau) + \bar{\chi}_2^A(\tau) = 1 \quad (35)$$

4. Values of problem parameters for typical arterial drug-delivery problem

While the two-layer drug delivery model discussed in Section 2 is quite general, and may be applicable to a number of distinct drug delivery scenarios, the specific focus of this work is on stent-based arterial dual drug delivery processes. We assume simultaneous diffusion and binding of two commonly used drugs – sirolimus and paclitaxel –denoted as Drugs A and B, respectively, in the model presented above. Each of these drugs has been heavily studied [20,21]. Paclitaxel is known to bind specifically to the subunit of tubulin present on microtubules, predominantly exerting its effect at the G2/M phase of the cell-cycle [22], while sirolimus is known to bind to cytosolic protein FKBP12, thereby hindering the functionality of FKBP-rapamycin-associated protein (FRAP) and affecting the mTOR pathway as a result of growth factor stimulation [23].

Values of various diffusion and binding coefficients for each drug are taken from past literature [6,9,16, 24-28], as summarized in Table 1. In some cases, these values are based on experimental measurements, while in others, the values have been estimated or inferred due to a lack of experimental data. Values of non-dimensional parameters are calculated based on these values, using equations (9) and (10). It is helpful to note a few key features of this baseline set of data. Firstly, the stent coating thickness is much smaller than that of the artery, so that γ_1 has a very small numerical value. This multiscale nature of the problem introduces stiffness in numerical computation. In order to mitigate this, an equal number of nodes are considered in each layer, so that the element size in the stent is much smaller than in the artery. In addition, a stiff numerical solver is used for computation.

Further, Table 1 shows that the diffusion coefficient of each drug in the stent layer is much lower than in the artery layer. As a result, the drugs are expected to diffuse very slowly in the stent, but diffuse much faster once the drug enters the artery. For the specific binding reaction, the forward reaction coefficient for sirolimus is significantly larger than for paclitaxel. In addition, the backward reaction coefficient for sirolimus is significantly smaller than for paclitaxel. As a result, sirolimus is expected to specifically bind much faster than paclitaxel, and, once bound, undergo the unbinding reaction much slower than paclitaxel. Specific binding reactions for sirolimus and paclitaxel occur independent of each other. For non-specific binding, where the two drugs compete with each other for a finite number of binding sites, data in Table 1 show that the forward reaction coefficient for sirolimus is larger than for paclitaxel. However, unlike specific binding, the backward reaction coefficient for sirolimus is larger than for paclitaxel. This implies that while sirolimus may exhibit greater tendency to non-specifically bind than paclitaxel, it will also unbind much faster than paclitaxel. The magnitudes of these reaction coefficients for the two drugs relative

to each other play a key role in determining the dynamics of drug uptake in the artery. This is discussed in more detail in subsequent sections.

6. Results and Discussion

6.1. Comparison with exact solutions of special cases:

It is of interest to compare the results of the numerical computation with exact solutions that may be derivable for simplified special cases of the general problem considered here. Two cases are considered here. In the first case, only irreversible binding of a single drug is considered in the two-layer geometry, i.e., the reverse reaction coefficients represented by $\bar{\sigma}$ are all zero for both layers. In such a case, the problem is completely uncoupled, and only the free drug concentrations $\bar{c}_1^A$ and $\bar{c}_2^A$ need to be solved, permitting an analytical solution can be derived, as outlined in Appendix A.

A second case of interest for comparison between numerical computation and an exact solution pertains to the case of pure diffusion, i.e., no drug binding at all, which may be modeled by setting all reaction coefficients $\bar{\sigma}$ and $\bar{\mu}$ to zero. The exact analytical solution for this problem is also derived in Appendix A.

A comparison of the numerically computed concentration field with the exact analytical solution for these special cases is carried out. Figures 2(a) and 2(b) present this comparison when a single drug undergoes irreversible binding or no binding at all in layer 2. The analytical solution is based on equations (A3)-(A4) as outlined in Appendix A, where $\bar{\beta}_1 = \bar{\beta}_2 = 0$ for the case of no binding at all. Figure 2 plots the free drug concentration distribution in a two-layer body at multiple

times, starting from uniform drug loading in layer 1 at the initial time. Values of problem parameters are $\overline{D}_1 = 0.4, \gamma_1 = 0.4$ and $\bar{\beta}_2 = 12.0$ for the irreversible binding case shown in Figure 2(a). Note that $\bar{\beta}_m = \mu_m^s B_m$, as defined in Appendix A. A zero concentration boundary is assumed at the $\xi = 1$. A total of 40 terms, verified separately to be sufficient to ensure converged results, is used for the exact series solution. Curves from the numerical calculations as well as the exact solution in Figure 2 show excellent agreement at each time for both cases. In general, the free drug concentrations in layer 2 for the case of no binding are greater than the case of irreversible binding, because in the latter case, free drug gets consumed over time.

A further comparison with exact solution is presented in Figure 3. Drug concentration at the middle of layer 2 is plotted as a function of time for four different values of the binding coefficient $\bar{\beta}_2$. Other parameters are the same as Figure 2. In each case, curves based on numerical calculations as well as the exact solution are plotted. There is excellent agreement between the two for each case considered here. Drug concentration at the center of layer 2 rises with time, reaches a peak and then decays away. As expected, the curve corresponding to the largest value of $\bar{\beta}_2$ shows the lowest drug concentration, which is due to greater consumption of drug in the irreversible binding reaction. These characteristics of curves shown in Figure 3 are consistent with the nature of diffusion, wherein, the point of interest first receives a large influx of drug from layer 1, but once the drug has diffused all the way to the right-hand boundary, significant drug loss begins to occur, particularly due to the zero concentration boundary condition, which explains the decaying nature of these curves at larger times. Note also for a very short initial time, the curves are nearly flat, which occurs because at very early times, drug is still diffusing from layer 1 towards the point of interest, during which time, there is no appreciable rise in drug concentration at the center of layer 2.

6.2. Overall mass balance

For the parameter values listed in Section 5.2, an overall mass balance for the problem is carried out. As outlined in section 3, for each drug separately, total amounts of free sirolimus and paclitaxel in layers 1 and 2, and bound drug – specifically or non-specifically –in layer 2 are calculated. The total amount of both drugs lost at the right surface ($\xi = 1$) are also calculated. Overall mass conservation of these quantities over time, per equation (34) is examined using parameter values listed in Table 1. In addition, the value of the Sherwood number is taken to be 0.1 for each drug throughout this work. Note that quantitative information about the Sherwood number is generally unavailable in the literature, and the assumed value quite likely corresponds to slow convective conditions at the boundary. For this set of parameters, Figure 4 plots the total amounts of free drug remaining in each layer, as well as specifically and non-specifically drug bound in layer 2. The total amount of drug lost to the surrounding medium at the convective boundary up to a given time is also plotted. Curves for sirolimus and paclitaxel are plotted in parts (a) and (b), respectively. Note that curves for drug bound in the stent coating layer are not plotted, since there is no drug uptake in the stent for the parameter values simulated. It is important to note that the total sum of these curves, also plotted in Figure 4(a) and 4(b) are found to be very close to 1 for both drugs, except for a small numerical error at early times, which is found to reduce with finer mesh discretization. This is consistent with equation (34) and demonstrates that the numerical calculations satisfy overall mass balance. This provides additional confidence in the accuracy of the numerical technique utilized in this work.

These plots show that as drug diffuses into the artery, the amount remaining in the stent coating layer reduces steadily. The free drug remaining in the artery increases initially, as more and more drug is received from the stent coating layer, while the drug has not yet diffused to the convective boundary. At later times, once drug begins to be lost at the convective boundary, the amount of drug remaining in the artery layer saturates and decreases very slowly over time. The amount of drug lost at the convective boundary is very small at early times, due to the large diffusive time scales and drug binding, but rises at later times. The plots for sirolimus and paclitaxel are broadly similar.

The amounts of drug bound specifically or non-specifically are both small relative to other quantities. This shows that the amount of drug bound in the artery is only a small fraction of the drug loaded in the stent. This is largely dependent on the specific values of key parameters governing binding and drug loss, such as binding site density, reaction coefficients and the Sherwood number. These important quantities are difficult to discern due to the scale in these plots, but are of interest from a safety and efficacy standpoint. As a result, these quantities are plotted separately in Figure 5, where the total non-specifically bound sirolimus and paclitaxel are plotted as functions of time in Figure 5(a) and total specifically bound sirolimus and paclitaxel are plotted as functions of time in Figure 5(b).

The effect of various problem parameters on the dynamics of drug binding is investigated in detail in subsequent sub-sections.

6.3. Dynamics of specific and non-specific two-drug binding

Sirolimus and paclitaxel undergo binding through two distinct mechanisms – non-specific binding, in which the two compete with each other for binding sites, and specific binding, in which the binding processes for the two drugs are independent of each other. The dynamics of non-specific binding is considered first.

Figure 6(a) plots non-specifically bound sirolimus concentration distributions in the artery at multiple times. A similar plot for paclitaxel is presented in Figure 6(b). These plots show that non-specifically bound sirolimus concentration is very high at small times, compared to paclitaxel. The sirolimus binding front moves right-wards with time, as shown in Figure 6(a). However, the concentration curves for sirolimus also drop off very rapidly at subsequent times. On the other hand, paclitaxel is slow to bind at initial times, but catches up with, and indeed exceeds, sirolimus at later times, as seen in total bound drug plots shown in Figure 5(a). At early times, most of the non-specific binding sites are occupied by sirolimus, whereas the competition for binding sites shifts more and more in favor of paclitaxel at larger times. This characteristic of non-specific binding may be explained on the basis of the values of non-specific forward and backward reaction coefficients for sirolimus and paclitaxel. While the forward reaction coefficient for sirolimus is one order of magnitude larger than paclitaxel, the backward coefficient for sirolimus is also one order of magnitude larger than paclitaxel. This is the reason why sirolimus dominates the competition for non-specific binding sites at early times. However, at later times, bound sirolimus also unbinds faster than paclitaxel, which is why, at later times, paclitaxel catches up with sirolimus, especially away from the convective boundary.

A similar comparison between the two drugs for specific binding is presented in Figure 7. Specifically bound sirolimus and paclitaxel concentration distributions are plotted as functions of

time in Figure 7(a) and 7(b), respectively. Figure 7(a) shows that specific binding of sirolimus occurs very rapidly, i.e., the diffusion of sirolimus from stent into the artery very quickly saturates specific sirolimus binding sites, following which, the binding front simply propagates towards the right over time.. After some time, nearly all available specific binding sites for sirolimus are occupied. Note that the peak value of 1 in the curves shown in Figure 7(a) indicate that all binding sites are occupied. This characteristic of sirolimus is consistent with the relative values of binding reaction coefficient. For specific binding reactions, the forward coefficient for sirolimus is five orders of magnitude larger than paclitaxel, which is why sirolimus is seen to saturate its specific binding sites so quickly. Moreover, the backward coefficient for sirolimus is three orders of magnitude smaller than paclitaxel, which is why sirolimus, once bound, does not appreciably unbind, and nearly all sirolimus binding sites remain occupied. On the other hand, due to more moderate values of forward and backward binding reaction coefficients, paclitaxel undergoes much more binding and unbinding, which is why, the paclitaxel concentration distribution fluctuates up and down with time, as seen in Figure 7(b) between curves corresponding to $\tau = 0.003, \tau = 0.03$ and $\tau = 0.3$. Unlike sirolimus, specific binding sites for paclitaxel are not fully occupied at small or large times.

6.4. Effect of initial drug distributions in stent

All analysis presented in prior sub-sections assumes uniform initial distribution of each drug in the stent coating layer, as shown schematically in Figure 1(b). Since the two drugs can potentially be embedded in the stent coating independent of each other, it is of interest to understand how the initial drug distributions in the stent coating affect drug diffusion and uptake over time. This is particularly important in the present problem due to the coupled nature of

sirolimus and paclitaxel uptake in non-specific binding sites. In order to investigate this further, numerical computation is carried out for three Cases illustrated in Figure 1(b). In Case I, both drugs are distributed uniformly in the stent. In Case II, sirolimus is loaded only in the left half (closest to the lumen) and paclitaxel is loaded only in the right half (closest to the tissue). In Case III, the initial distribution is flipped, so that sirolimus and paclitaxel are loaded only in the right and left half, respectively. The total amount loaded remains the same in the three Cases, for both sirolimus and paclitaxel, to facilitate comparison between the three Cases. These Cases, illustrated in Figure 1(b) may be used to understand how such relative positioning of the drugs affects uptake.

In order to understand this further, Figure 8 plots free drug distributions for all three Cases at multiple times, including at the initial time. Due to the significant difference in length scales of the stent and artery, distributions in the two layers are presented separately in Figures 8(a) and 8(b), respectively. The initial drug distribution for the three Cases can be easily visualized in the τ=0 curves in Figure 8(a). It is seen in Figure 8(a) that for the baseline case of uniform drug distribution, the free drug distribution in the stent coating decreases slowly over time, starting from the right end of the stent, as the drug diffuses into the artery. For Case III, in which, sirolimus is loaded only in the second half of the stent, located next to the artery, the drug distribution exhibits a non-monotonic behavior, which may be because of much faster sirolimus diffusion into the artery, within which, sirolimus diffuses even faster once entered. This results in a rapid reduction in sirolimus concentration in stent regions very close to the artery, but farther away from the stent-artery interface, the sirolimus concentration reduces due to diffusion towards the left since the first half of the artery does not initially contain sirolimus. Between these two diffusion processes causing sirolimus depletion, at τ=0.5, there appears a peak in sirolimus concentration at a point

that remains relatively unaffected by both. The peak, however, disappears at larger times, when reduction in sirolimus concentration due to diffusion into the artery dominates.

Figure 8(b) plots free drug distributions in the artery at multiple times for the three Cases. In general, drug concentration in the artery increases with time in each Case, due to increased diffusion of the drug from the stent. In Case II, where sirolimus is loaded away from the artery, there is reduced drug in the artery at small times, but at larger times, Case II catches up with Case I, so that the curves for tau=10 are similar for these two Cases. Free sirolimus available in the artery is modestly larger for Case III, in which, sirolimus is loaded only on the artery-facing half of the stent coating, compared to the other two Cases, as seen in the third plot in Figure 8(b).

The impact of initial drug distribution on drug binding in the artery is examined next. Figure 9(a) plots total amount of drug bound, both specifically and non-specifically, as a function of time for the three Cases. Figure 9(a) shows that for the fast diffusing and fast binding sirolimus, the bound drug concentration curves for Cases I and III peak very quickly due to faster diffusion of sirolimus into the artery and subsequent saturation of binding sites. However, this does not occur for Case II, in which, sirolimus is loaded in the left half of the stent, away from the stent, due to which, it takes a longer time for sirolimus to diffuse into the artery. The opposite trend is seen for Paclitaxel, as expected. When Paclitaxel is loaded close to the artery (Case II), Figure 9(a) shows rapid binding of paclitaxel due to faster diffusion into the artery, relative to sirolimus. In this case, Paclitaxel dominates over sirolimus for non-specific binding at early times due to greater availability. On the other hand, when Paclitaxel is loaded away from the artery (Case III), there is less binding of Paclitaxel, especially at early times. These observations indicate that the relative distribution of drug in the stent has a profound impact on the dynamics of binding in the artery.

Therefore, the relative distribution of drug in the stent can potentially be used to achieve a desirable binding profile in the artery.

The impact of initial drug distribution on drug lost from the right side boundary is examined in Figure 9(b). Compared to the baseline Case I, there is lower and greater sirolimus lost in Cases II and III, respectively, due to the sirolimus being loaded away from and next to the artery in these Cases, respectively. Similar observations along expected lines can be made for paclitaxel. Note that the amount of drug lost is also likely to be a strong function of the Sherwood number, as it governs the nature of the convective boundary.

Figure 10 plots total free sirolimus concentration for the three Cases. For Cases I and III, in which sirolimus is loaded uniformly and in the artery-facing half of the stent coating, respectively, the curves in Figure 10 rise rapidly at initial time, because sirolimus is available to diffuse into the artery starting at the initial time. In contrast, when sirolimus is loaded in the half of the stent away from the artery (Case II), the curve is slow to rise at early time, which is because it takes a finite amount of time for sirolimus to diffuse through the stent and then enter the artery. Free drug concentrations in Cases I and II reach a peak and then slowly go down, because of consumption of the drug in binding reactions.

7. Conclusions

A number of physical processes contribute towards the complexity of endovascular drug delivery, including diffusion and binding, which may be specific or non-specific, as well as reversible or irreversible. This problem is made even more complicated by the simultaneous delivery of multiple drugs. In order to maximize the therapeutic benefits of dual-drug delivery, the key contribution of this work is in the development of a rigorous and general numerical

computation model. Key insights gained from this work include the importance of relative values of diffusion coefficients and binding reaction coefficients of the two drugs, as well as the nature of competitive non-specific binding in determining dual drug uptake. Further, the role of initial distribution of the two drugs in determining drug uptake as a function of time may be of much practical interest, for example, in determining drug distribution strategies to meet desirable drug uptake goals. Such insights can be used to balance safety and efficacy of dual drug delivery.

While the model is formulated in a very general fashion, nevertheless, it is important to recognize key underlying assumptions. The artery is modeled as a homogeneous material, although extension of the present work to account for multilayer nature of the artery is quite straightforward. Convective flow and the resulting mass transfer due to transvascular pressure is neglected. This assumption is valid in cases where the arterial Péclet number (*Pe*) is less than 1, in which case diffusion dominates over advection. Further, it is assumed that the application of the stent does not influence local geometry or properties of the artery. Based on past work, these assumptions may be reasonable in a broad range of parameters. Finally, the predictive accuracy of the numerical model depends critically on the accuracy of values of underlying parameters. While these parameter values have been obtained from past work, more detailed measurements in a variety of arterial conditions may be beneficial. Moreover, it is hoped that this work will inspire experimental measurements that would facilitate validation of the mathematical model.

This work contributes towards an improved mathematical understanding of a promising dual-drug delivery technique, which may be useful for design and optimization. While discussed here in the context of endovascular drug delivery, the numerical model is equally applicable for other drug delivery problems, with appropriately chosen parameter values.

Acknowledgments

Funding from the European Research Council under the European Union Horizon 2020 Framework Programme (No. FP/2014-2020) ERC Grant Agreement No. 739964 (COPMAT) is acknowledged. This work is also partially supported by Italian MIUR (PRIN 2017 project: Mathematics of active materials: from mechanobiology to smart devices, project number 2017KL4EF3).

Conflict of Interest Statement

The authors declare that they do not have any conflict of interest related to this work.

REFERENCES

[1] Mcginty, S., Pontrelli, G., 'A general model of coupled drug release and tissue absorption for drug delivery devices,' *J. Control. Release*, **217**, pp. 327-336, 2015. DOI: 10.1016/j.jconrel.2015.09.025

[2] Jain, A., McGinty, S., Pontrelli, G., 'Theoretical Modeling of Endovascular Drug Delivery into a Multilayer Arterial Wall from a Drug-Coated Balloon,' *Int. J. Heat Mass Transfer*, **187**, pp. 122572:1-17, 2022. DOI: 10.1016/j.ijheatmasstransfer.2022.122572.

[3] d'Errico, M., Sammarco, P., Vairo, G., 'Analytical modeling of drug dynamics in- duced by eluting stents in the coronary multi-layered curved domain,' *Math. Biosci.*, **267**, pp. 79–96, 2015. DOI: 10.1016/j.mbs.2015.06.016

[4] McKittrick, C., McKee, S., Kennedy, S., et al., 'Combining mathematical modeling with in vitro experiments to predict in vivo drug-eluting stent performance,' *J. Control. Release*, **303**, pp. 151-161, 2019. DOI: 10.1016/j.jconrel.2019.03.012

[5] Bozsak, F., Gonzalez-Rodriguez, D., Sternberger, Z., et al., 'Optimization of drug delivery by drug-eluting stents,' *PLoS One*, **10**, pp. e0130182, 2015. DOI: 10.1371/journal.pone.0130182

[6] Mcginty, S., Pontrelli, G., 'On the role of specific drug binding in modeling arterial eluting stents,' *J. Mathemat. Chem.*, **54**, pp. 967-976, 2016. DOI: 10.1007/s10910-016-0618-7

[7] McHugh, P., Barakat, A., Mcginty, S. (Eds.), 'Medical Stents: State of the Art and Future Directions,' *Annals Biomed. Eng.*, **44**, pp. 274-275, 2016. DOI: 10.1007/s10439-015-1526-x

[8] Hwang, C.-W., Wu, D., Edelman, E.R., 'Impact of transport and drug properties on the local pharmacology of drug-eluting stents,' *Int. J. Cardiovasc. Intervent.*, **5**, pp. 7-12, 2009. DOI: 10.1080/14628840304614

[9] Tzafriri, A.R., Groothuis, A., Price, G.S., Edelman, E.R., 'Stent elution rate determines drug deposition and receptor-mediated effects,' *J. Control. Release*, **161**, pp. 918-926, 2012. DOI: 10.1016/j.jconrel.2012.05.039

[10] Ma, X., Oyamada, S., Gao, F., et al., 'Paclitaxel/sirolimus combination coated drug-eluting stent: In vitro and in vivo drug release studies,' *J. Pharm. Biomed. Anal.*, **54**, pp. 807-811, 2011. DOI: 10.1016/j.jpba.2010.10.027

[11] Lei, L, Guo, S.-R., Chen, W.-L., Rong, H.-J., Lu, F., 'Stents as a platform for drug delivery,' *Expert Opinion Drug. Deliv.*, **8**, pp. 813-831, 2011. DOI: 10.1517/17425247.2011.572068

[12] Byrne, R.A., Mehilli, J., Iijima, R., et al., 'A polymer-free dual drug-eluting stent in patients with coronary artery disease: a randomized trial vs. polymer-based drug-eluting stents,' *Eur. Heart J.*, **30**, pp. 923–931, 2009. DOI:10.1093/eurheartj/ehp044

[13] Roopmani, P., Satheesh, S., Raj, D.C., Krishna, U.M., 'Development of Dual Drug Eluting Cardiovascular Stent with Ultrathin Flexible Poly(l-lactide-co-caprolactone) Coating,' *ACS Biomater. Sci. Eng.*, **5**, 2899–2915, 2019. DOI: 10.1021/acsbiomaterials.9b00303

[14] Cha, J.-J., Kim, G.-C., Hur, S.-H., 'Efficacy and Safety of Dual-Drug-Eluting Stents for de Novo Coronary Lesions in South Korea—The Effect Trial', *J. Clinic. Med.*, **10**, pp. 69:1-9, 2021, DOI: 10.3390/jcm10010069

[15] Huang, Y., Venkatraman, S.S., Boey, F.Y.C., et al., 'In vitro and in vivo performance of a dual drug-eluting stent (DDES),' *Biomater.*, **31**, pp. 4382-4391, 2010. DOI:10.1016/j.biomaterials.2010.01.147

[16] Escuer, J., Schmidt, A.F., Peña, E., Martínez, M.A., McGinty, S., 'Mathematical modelling of endovascular drug delivery: Balloons versus stents,' *Int. J. Pharmceut.*, **620**, pp. 121742, 2022. DOI: 10.1016/j.ijpharm.2022.121742

[17] Escuer, J., Aznar, I., McCormick, C., Peña, E., McGinty, S., Martínez, M.A. 'Influence of vessel curvature and plaque composition on drug transport in the arterial wall following drug-eluting stent implantation,' *Biomech. Modeling Mechanobiol.*, **20**, pp. 767-786, 2021. DOI: 10.1007/s10237-020-01415-3.

[18] Hickson, R.I., Barry, S.I., Mercer, G.N., Sidhu, H.S., 'Finite difference schemes for multilayer diffusion,' *Mathemat. & Comput. Model.*, **54**, pp. 210-220, 2011. DOI: 10.1016/j.mcm.2011.02.003

[19] https://www.mathworks.com/help/matlab/ref/ode23s.html, last accessed 06/21/2022.

[20] Ma, P., Mumper, R.J., 'Paclitaxel Nano-Delivery Systems: A Comprehensive Review,' J. Nanomed. Nanotechnol., 4, pp. 1000164, 2013. DOI: 10.4172/2157-7439.1000164

[21] Kahan, B.D., 'Sirolimus: a comprehensive review,' Exp. Opin. Pharmacotherap., 2, pp. 1903-1917, 2001. DOI: 10.1517/14656566.2.11.1903

[22] Oberhoff, M., Herdeg, C., Baumbach, A., Karsch, K.R., 'Stent-based antirestenotic coatings (sirolimus/paclitaxel),' *Catheter. Cardiovasc. Intervent.*, **55,** pp. 404-408, 2002. DOI: 10.1002/ccd.10034[23] Wessely, R., Schomig, A. Kastrati, A., 'Sirolimus and paclitaxel on polymer-based drug-eluting stents,' *J. Am. Coll. Cardiol.*, **47**, pp. 708-714, 2006. DOI: 10.1016/j.jacc.2005.09.047.[24] Levin, A.D., Vukmirovic, N., Hwang, C.-W., Edelman, E.R., 'Specific binding to intracellular proteins determines arterial transport properties for rapamycin and paclitaxel,' *Proc. Natl. Acad. Sci. USA*, **101**, pp. 9463-9467, 2004. DOI: 10.1073/pnas.0400918101

[25] Díaz, J.F., Barasoain, I., Andreu, J.M., 'Fast kinetics of taxol binding to microtubules effects of solution variables and microtubule-associated proteins,' *J. Biol. Chem.*, **278**, pp. 8407-8419, 2003. DOI: 10.1074/jbc.M211163200

[26] Wear, M.A., Walkinshaw, M.D., 'Determination of the rate constants for the fk506 binding protein/rapamycin interaction using surface plasmon resonance: An alternative sensor surface for ni2+–nitrilotriacetic acid immobilization of his-tagged proteins,' *Anal. Biochem.*, **371**, pp. 250-252, 2007. DOI: 10.1016/j.ab.2007.06.034

[27] Escuer, J., Cebollero, M., Peña, E., McGinty, S., Martínez, M.A., 'How does stent expansion alter drug transport properties of the arterial wall?,' *J. Mech. Behav. Biomed. Mater.*, Article 103610, 2020. DOI: 10.1016/j.jmbbm.2019.103610

[28] Tzafriri, A.R., Levin, A.D., Edelman, E.R., 'Diffusion-limited binding explains binary dose response for local arterial and tumour drug delivery,' *Cell Prolif.*, **42**, pp. 348-363, 2009. DOI: 10.1111/j.1365-2184.2009.00602.x

Appendix A: Exact Solution for Irreversible Single Drug Binding in Two Layer Geometry

This Appendix derives an exact solution for two special cases of the general model, for comparison with numerical computations.

A.1. Special case of diffusion and irreversible binding of a single drug

First, diffusion and irreversible binding of a single drug in a two-layer geometry is considered. For simplicity, subscript A is dropped from the derivation below. In this case, it is assumed that the binding site density, $B_{max,m}$ is much larger than the concentration of bound drug, and therefore, the problem defined by equations ()-() in non-dimensional form can be linearized as follows:

$$\frac{\partial \bar{c}_1}{\partial \tau} = \bar{D}_1 \frac{\partial^2 \bar{c}_1}{\partial \xi^2} - \bar{\beta}_1 \bar{c}_1 \qquad 0 < \xi < \gamma_1 \text{ (A.1)}$$

$$\frac{\partial \bar{c}_2}{\partial \tau} = \frac{\partial^2 \bar{c}_2}{\partial \xi^2} - \bar{\beta}_2 \bar{c}_2 \qquad \gamma_1 < \xi < 1 \text{ (A.2)}$$

where $\bar{\beta}_m = \mu_m^s B_m$ for m=1,2, following linearization.

The associated boundary and interface conditions are given by equations ()-() in section 2.

Due to the linearization of this problem, an exact solution may be derived using the method of separation of variables. One may write the solution in the following form

$$\bar{c}_1(\xi, \tau) = \sum_{n=1}^{\infty} p_n \left[A_n \cos\left(\omega_{1,n}\xi\right)\right] \exp\left(-\lambda_n^2 \tau\right) \qquad \text{(A.3)}$$

$$\bar{c}_2(\xi, \tau) = \sum_{n=1}^{\infty} p_n \left[B_n \sin\left(\omega_{2,n}(1-\xi)\right)\right] \exp\left(-\lambda_n^2 \tau\right) \qquad \text{(A.4)}$$

Note that sine and cosine terms are not included in equations (A.3) and (A.4), respectively, in order to satisfy the boundary conditions at $\xi = 0$ and $\xi = 1$. In addition, in order for equations (A.3) and (A.4) to satisfy the governing equations given by equations () and () in section 2, one must have

$$\omega_{1,n} = \sqrt{\frac{\lambda_n^2 - \bar{\beta}_1}{\bar{D}_1}};\ \omega_{2,n} = \sqrt{\lambda_n^2 - \bar{\beta}_2} \qquad \text{(A.5)}$$

Further, in order for equations (A.3) and (A.4) to satisfy the interface conditions, one must require

$$A_n \cos(\omega_{1,n}\gamma_1) = B_n \sin\left(\omega_{2,n}(1-\gamma_1)\right) \tag{A.6}$$

$$-\bar{D}_1\omega_{1,n}A_n \sin(\omega_{1,n}\gamma_1) = -\omega_{2,n}B_n \cos\left(\omega_{2,n}(1-\gamma_1)\right) \tag{A.7}$$

Dividing equation (A.6) by (A.7), and rearranging, one may derive the following eigenequation to determine the eigenvalues λ_n:

$$\omega_{2,n} \cot\left(\omega_{2,n}(1-\gamma_1)\right) - \bar{D}_1\omega_{1,n} \tan(\omega_{1,n}\gamma_1) = 0 \tag{A.8}$$

Also, without loss of generality, one may assume $A_n = 1$ and obtain, from equation (A.6), $B_n = \frac{\cos(\omega_{1,n}\gamma_1)}{\sin\left(\omega_{2,n}(1-\gamma_1)\right)}$.

Finally, the remaining constants p_n may be obtained using the principle of orthogonality for a two-layer body as follows:

$$p_n = \frac{\int_0^{\gamma_1} c_{1,in}(\xi)\cos(\omega_{1,n}\xi)\,d\xi + \int_{\gamma_1}^{1} c_{2,in}(\xi)\frac{\cos(\omega_{1,n}\gamma_1)}{\sin\left(\omega_{2,n}(1-\gamma_1)\right)}\sin\left(\omega_{2,n}(1-\xi)\right)d\xi}{\int_0^{\gamma_1}\left[\cos(\omega_{1,n}\xi)\right]^2 d\xi + \int_{\gamma_1}^{1}\left[\frac{\cos(\omega_{1,n}\gamma_1)}{\sin\left(\omega_{2,n}(1-\gamma_1)\right)}\sin\left(\omega_{2,n}(1-\xi)\right)\right]^2 d\xi} \tag{A.9}$$

This completes the exact solution for the special case of irreversible drug binding in a two-layer body, with which, the numerical solution may be compared.

A.2. Special case of pure diffusion of a single drug

The exact solution for the case of pure diffusion of a single drug in a two-layer geometry can be easily obtained from the derivation above by setting $\bar{\beta}_1 = \bar{\beta}_2 = 0$ in equation (A.5), resulting in $\omega_{1,n} = \lambda_n/\sqrt{\bar{D}_1}$; $\omega_{2,n} = \lambda_n$. The rest of the solution is identical to the one presented in the previous section.

List of Figures:

Figure 1: (a) Schematics of specific vs. non-specific, and non-reversible vs reversible binding processes; (b) Schematic of the two-layer two-drug problem with reversible binding on both specific and non-specific binding sites, along with illustrations of three candidate initial distributions of drugs A and B in layer 1, referred to as Cases I, II and III.

Figure 2 – Comparison of numerical model with exact solution for the special cases of (a) no binding and (b) irreversible binding of a single drug. In each case, numerical model and exact solution are compared with each other in terms of concentration profiles at multiple times. The drug is uniformly loaded in layer 1 at the initial time.

Figure 3 – Comparison of numerical model with exact solution for the special case of irreversible binding of a single drug: Concentration profiles at the center of layer 2 as functions of time for multiple values of $\bar{\beta}_2$. The drug is uniformly loaded in layer 1 at the initial time.

(REVISED) Figure 4 – Plots of total amounts of free drugs in layers 1 and 2, $\bar{\rho}_1^A$ and $\bar{\rho}_2^A$, specifically and non-specifically bound drug in layer 2, $\bar{\psi}_2^{A,s}$ and $\bar{\psi}_2^{A,ns}$, and drug lost to the surrounding medium, $\bar{\chi}_2^A$ as functions of time for a baseline set of parameters. The total sum of these amounts is also plotted. (a) and (b) present plots for sirolimus and paclitaxel, respectively.

Figure 5 – Total bound sirolimus and paclitaxel in artery as functions of time: (a) Non-specifically bound quantities, $\bar{\psi}_2^{A,ns}$ and $\bar{\psi}_2^{B,ns}$, and (b) specifically bound quantities, $\bar{\psi}_2^{A,s}$ and $\bar{\psi}_2^{B,s}$ as functions of time. Both sirolimus and paclitaxel are assumed to be initially uniformly distributed in the stent. Other parameter values are listed in Table 1.

(REVISED) Figure 6 – Plots of non-specifically bound drug concentration distribution at different times for (a) sirolimus and (b) paclitaxel. Data are presented as a fraction of total number of binding sites. Both drugs are assumed to be uniformly distributed in layer 1 at the initial time. Other parameter values are listed in Table 1.

Figure 7 – Plots of specifically bound drug concentration distribution at different times for (a) sirolimus; and (b) paclitaxel. Data are presented as a fraction of total number of binding sites. Both

drugs are assumed to be uniformly distributed in layer 1 at the initial time. Other parameter values are listed in Table 1.

Figure 8 – Effect of initial drug distributions: Free sirolimus concentration distribution in (a) stent, and (b) artery at multiple times for the three cases illustrated in Figure 1(b).

Figure 9 – Effect of initial distributions of sirolimus and paclitaxel: (a) Total bound sirolimus and paclitaxel as functions of time, and (b) Total sirolimus and paclitaxel lost from the right boundary as functions of time. Both plots show curves corresponding to Cases I, II and III illustrated in Figure 1(b).

Figure 10 – Effect of initial drug distribution: Free sirolimus concentration as functions of time for three Cases I, II and III illustrated in Figure 1(b).

List of Tables

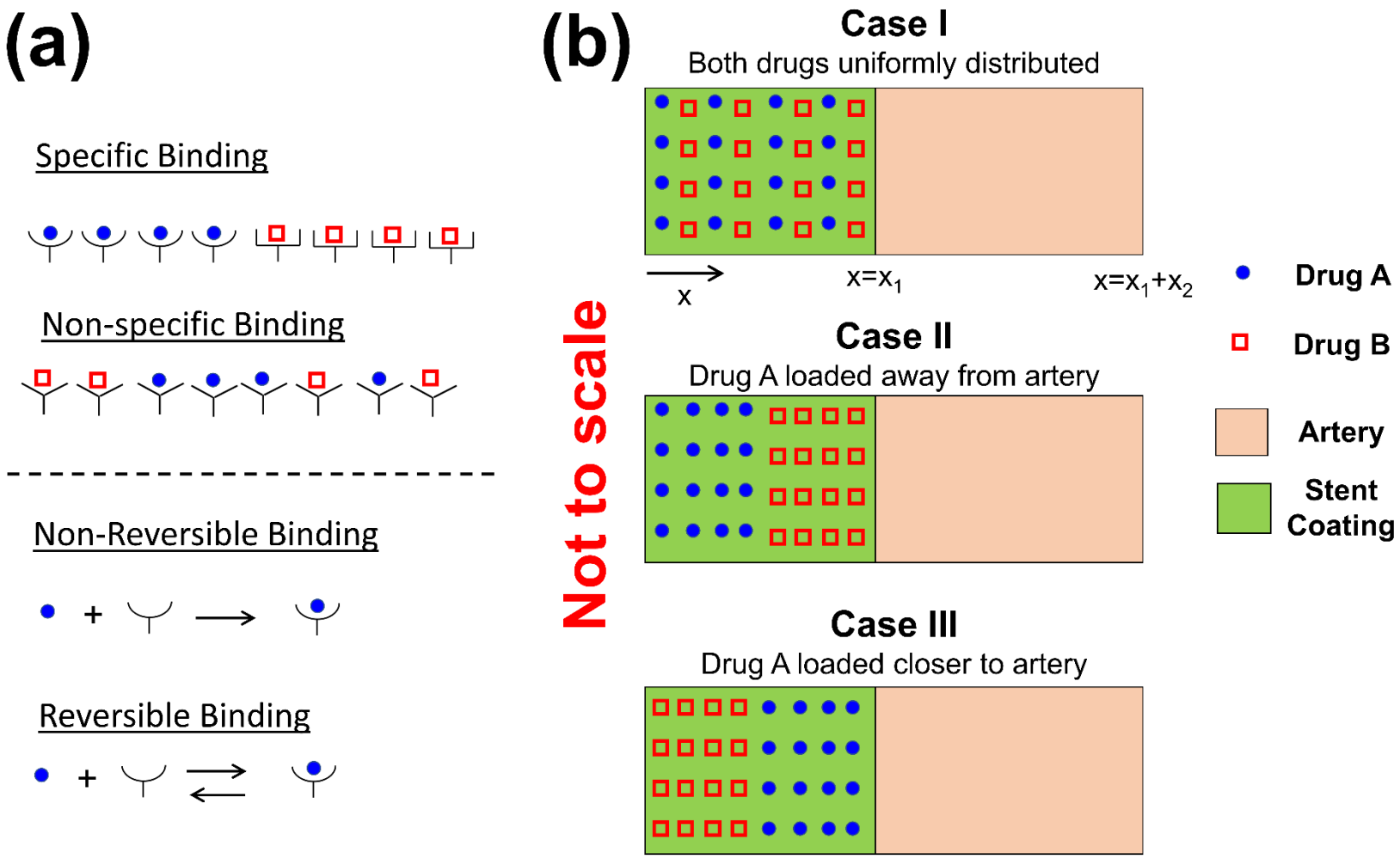

Figure 1: (a) Schematics of specific vs. non-specific, and non-reversible vs reversible binding processes; (b) Schematic of the two-layer two-drug problem with reversible binding on both specific and non-specific binding sites, along with illustrations of three candidate initial distributions of drugs A and B in layer 1, referred to as Cases I, II and III.

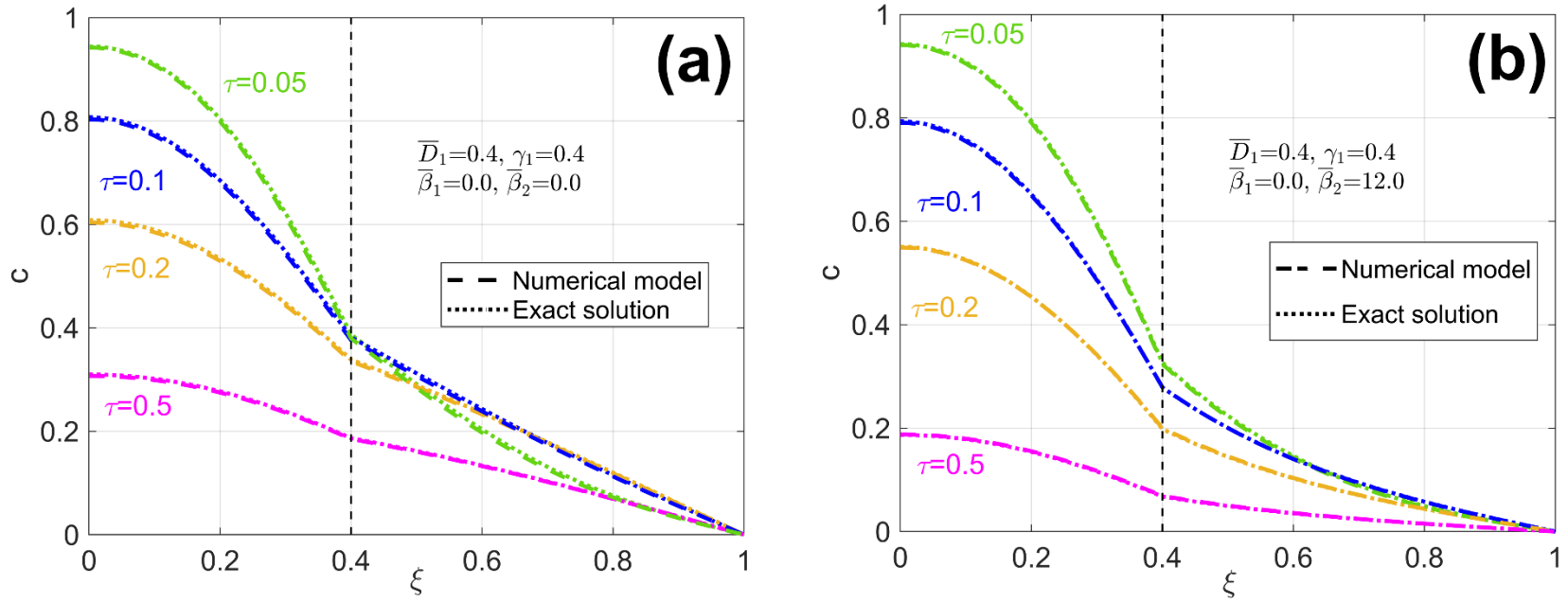

Figure 2 – Comparison of numerical model with exact solution for the special cases of (a) no binding and (b) irreversible binding of a single drug. In each case, numerical model and exact solution are compared with each other in terms of concentration profiles at multiple times. The drug is uniformly loaded in layer 1 at the initial time.

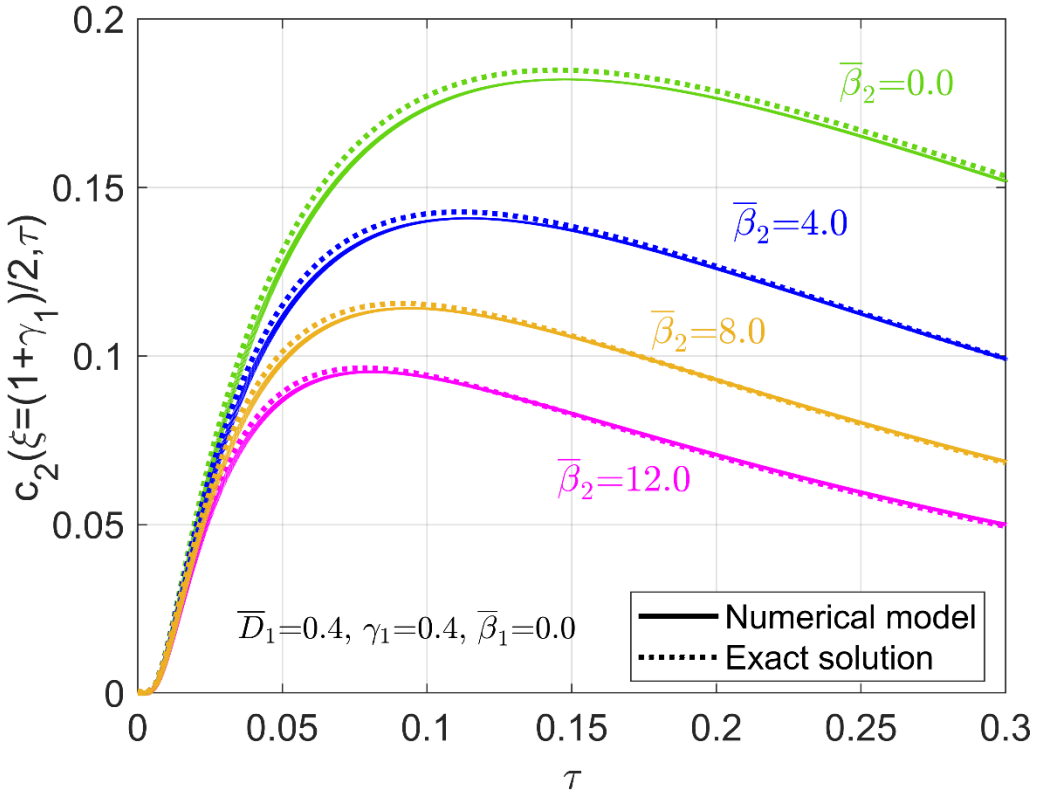

Figure 3 – Comparison of numerical model with exact solution for the special case of irreversible binding of a single drug: Concentration profiles at the center of layer 2 as functions of time for multiple values of $\bar{\beta}_2$. The drug is uniformly loaded in layer 1 at the initial time.

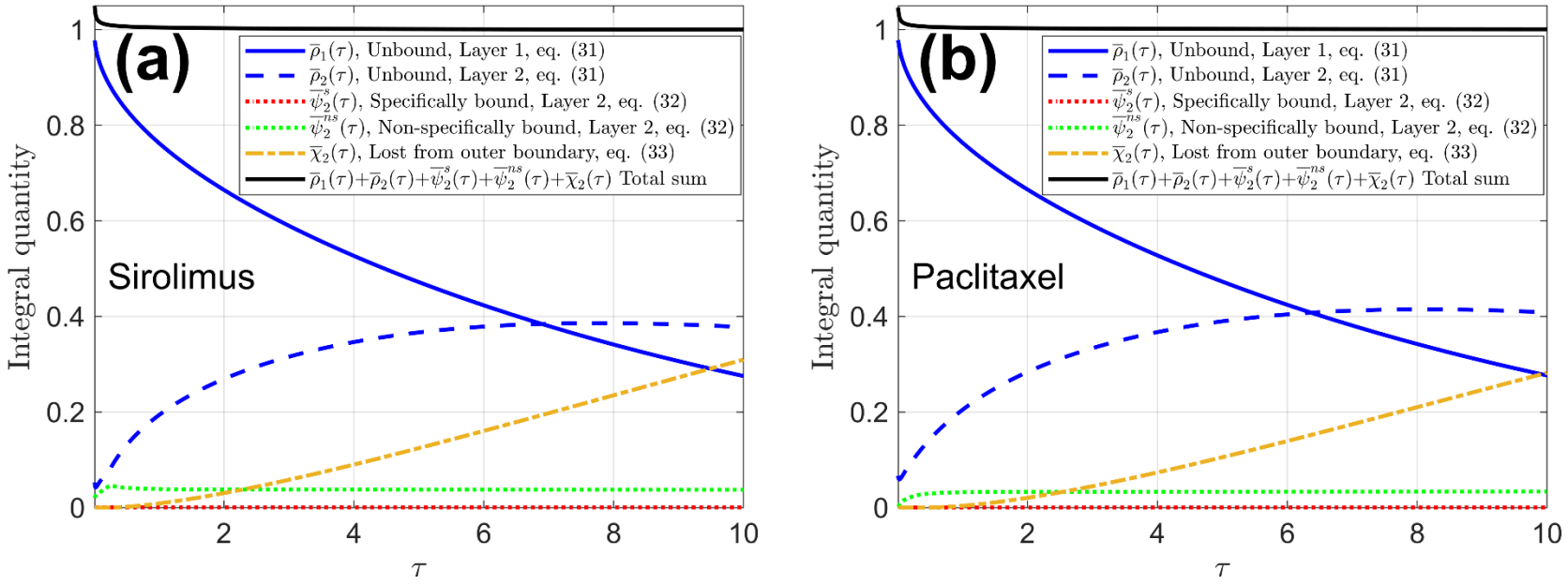

(REVISED) Figure 4 – Plots of total amounts of free drugs in layers 1 and 2, $\bar{\rho}_1^A$ and $\bar{\rho}_2^A$, specifically and non-specifically bound drug in layer 2, $\bar{\psi}_2^{A,s}$ and $\bar{\psi}_2^{A,ns}$, and drug lost to the surrounding medium, $\bar{\chi}_2^A$ as functions of time for a baseline set of parameters. The total sum of these amounts is also plotted. (a) and (b) present plots for sirolimus and paclitaxel, respectively.

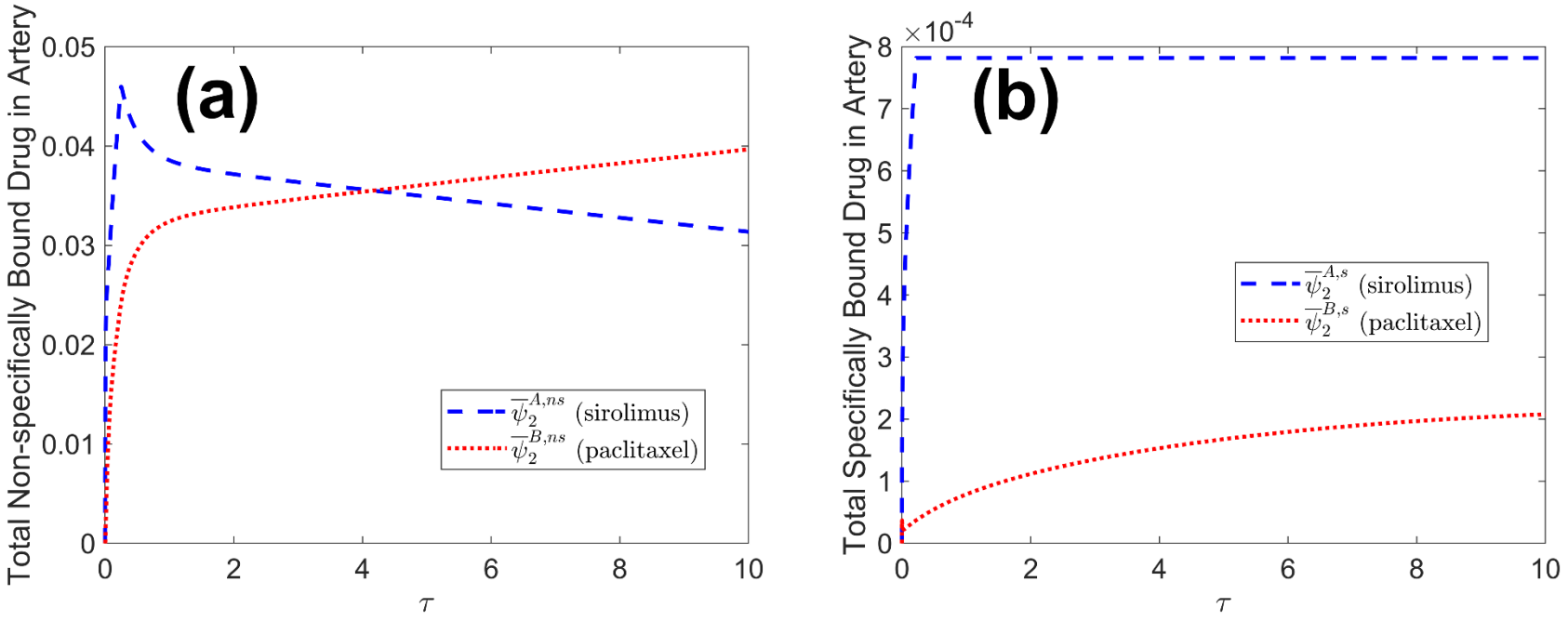

Figure 5 – Total bound sirolimus and paclitaxel in artery as functions of time: (a) Non-specifically bound quantities, $\bar{\psi}_2^{A,ns}$ and $\bar{\psi}_2^{B,ns}$, and (b) specifically bound quantities, $\bar{\psi}_2^{A,s}$ and $\bar{\psi}_2^{B,s}$ as functions of time. Both sirolimus and paclitaxel are assumed to be initially uniformly distributed in the stent. Other parameter values are listed in Table 1.

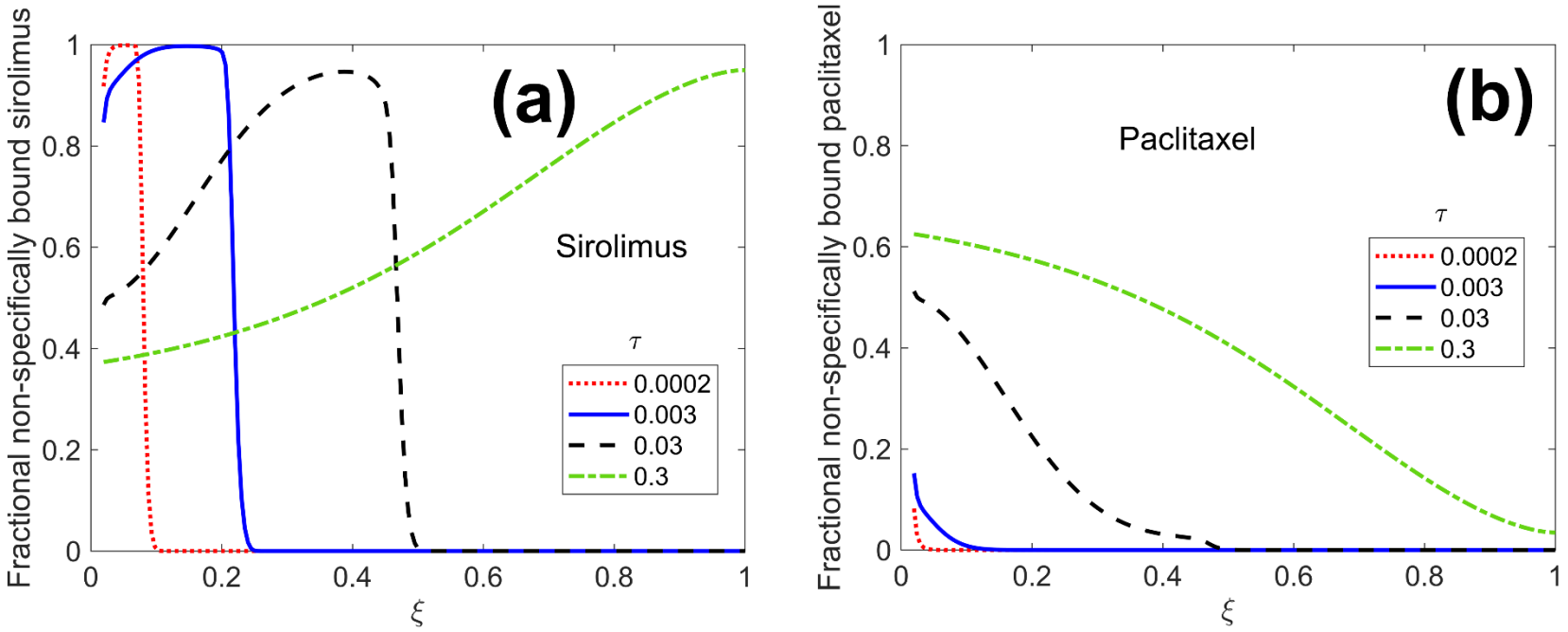

(REVISED) Figure 6 – Plots of non-specifically bound drug concentration distribution at different times for (a) sirolimus and (b) paclitaxel. Data are presented as a fraction of total number of binding sites. Both drugs are assumed to be uniformly distributed in layer 1 at the initial time. Other parameter values are listed in Table 1.

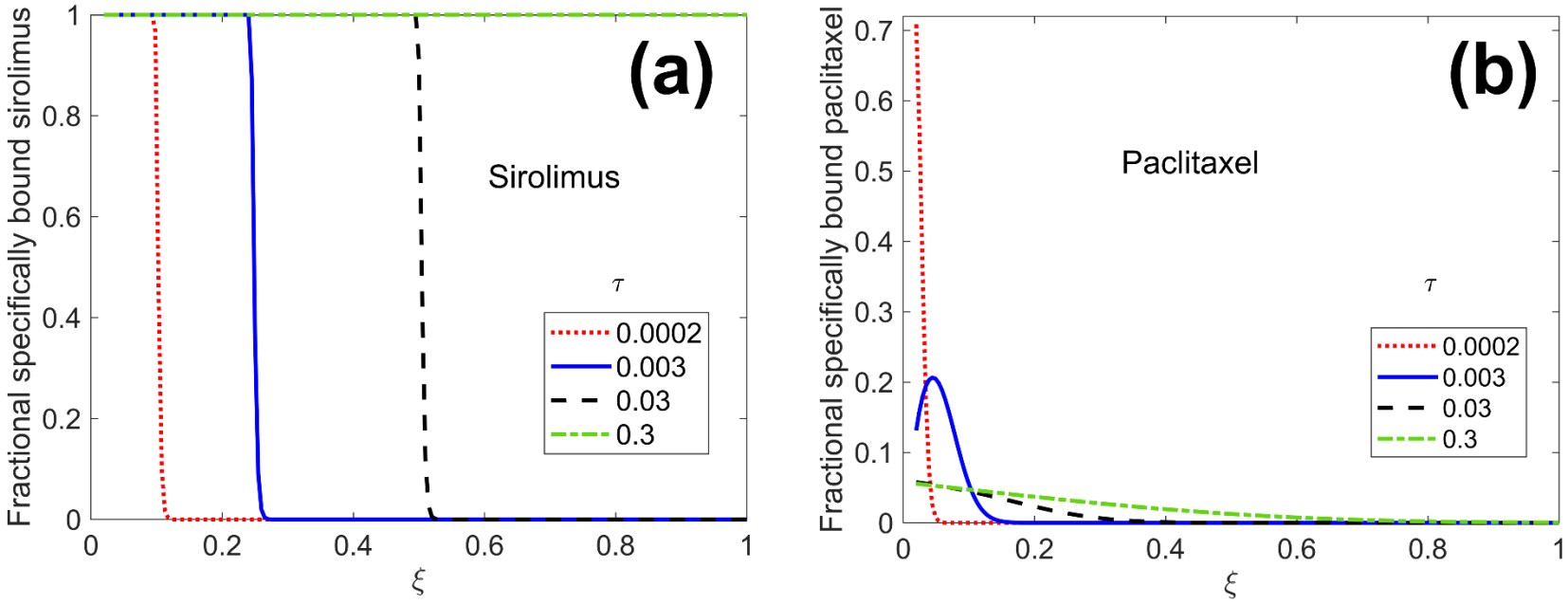

Figure 7 – Plots of specifically bound drug concentration distribution at different times for (a) sirolimus; and (b) paclitaxel. Data are presented as a fraction of total number of binding sites. Both drugs are assumed to be uniformly distributed in layer 1 at the initial time. Other parameter values are listed in Table 1.

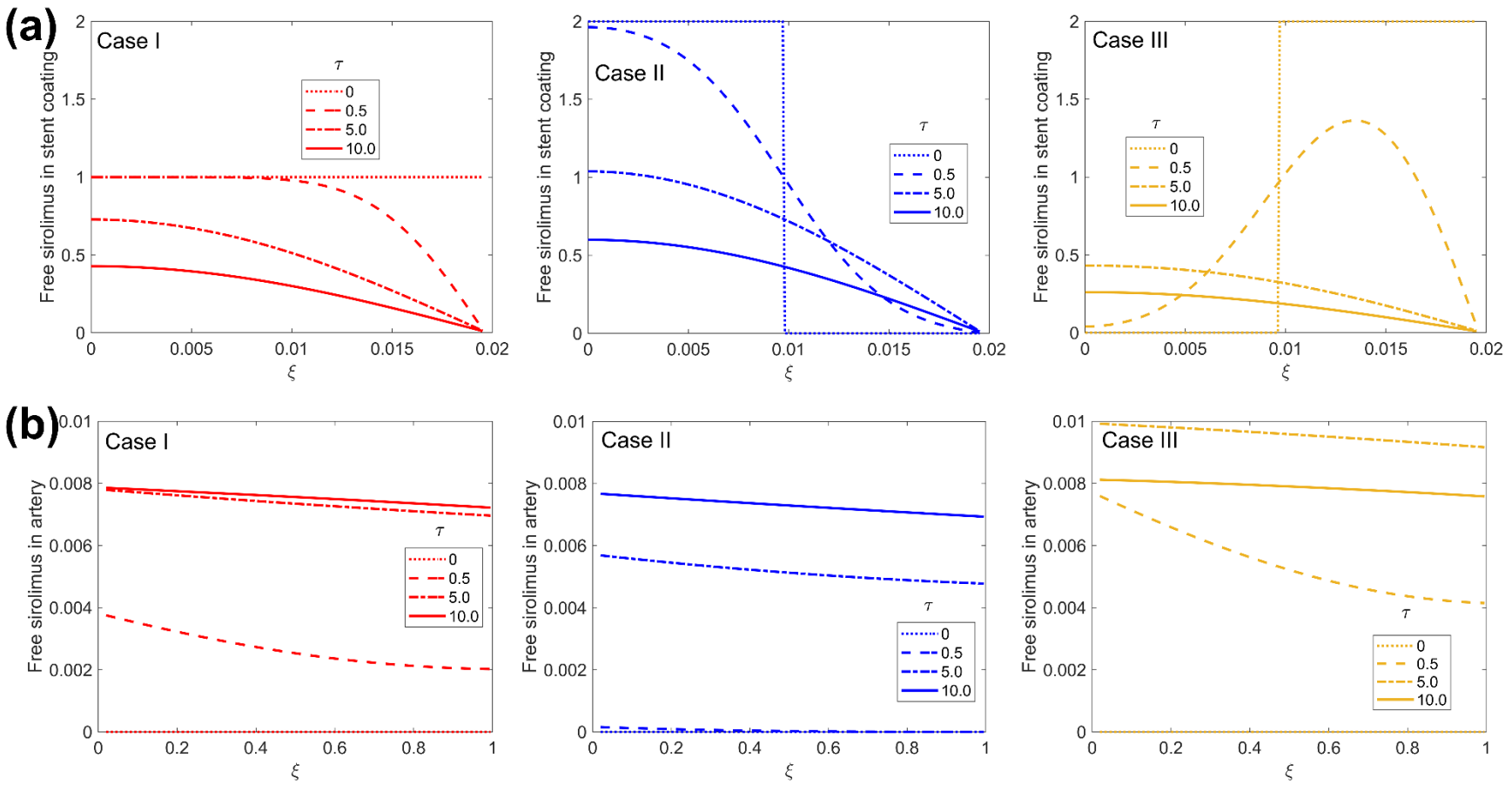

Figure 8. Effect of initial drug distributions: Free sirolimus concentration distributions in (a) stent, and (b) artery at multiple times for the three cases illustrated in Figure 1(b).

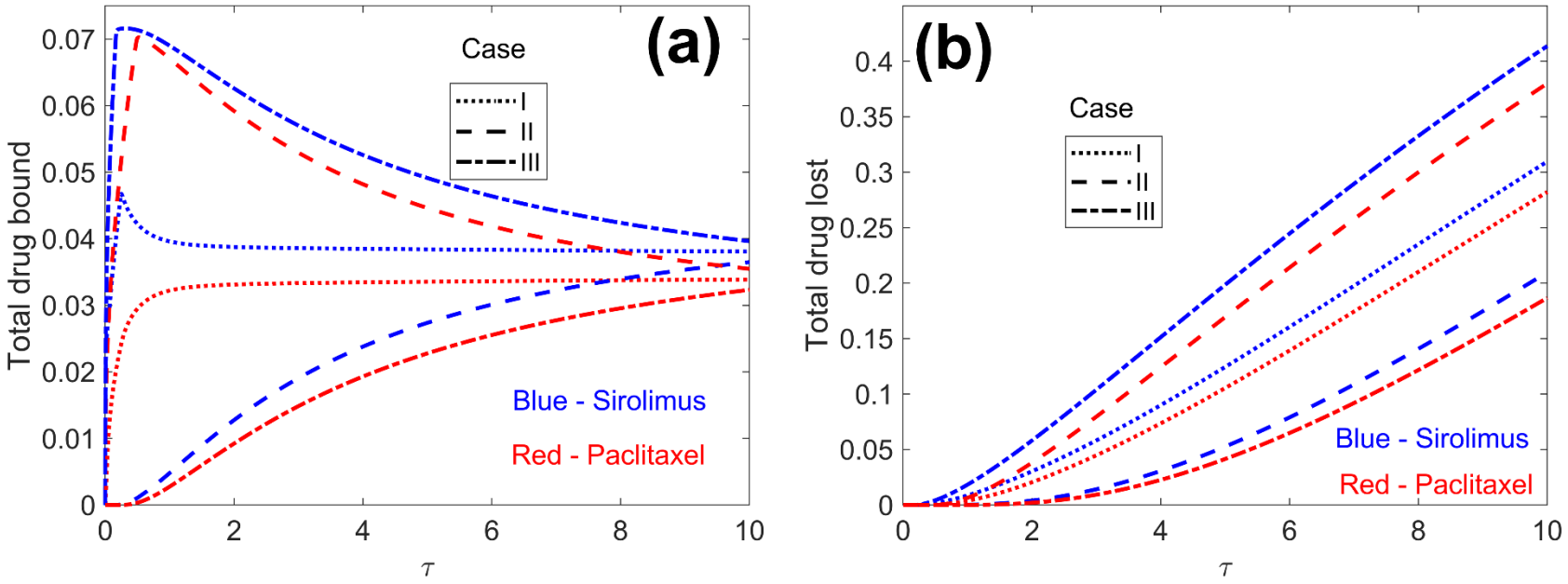

Figure 9 – Effect of initial distributions of sirolimus and paclitaxel: (a) Total bound sirolimus and paclitaxel as functions of time, and (b) Total sirolimus and paclitaxel lost from the right boundary as functions of time. Both plots show curves corresponding to Cases I, II and III illustrated in Figure 1(b).

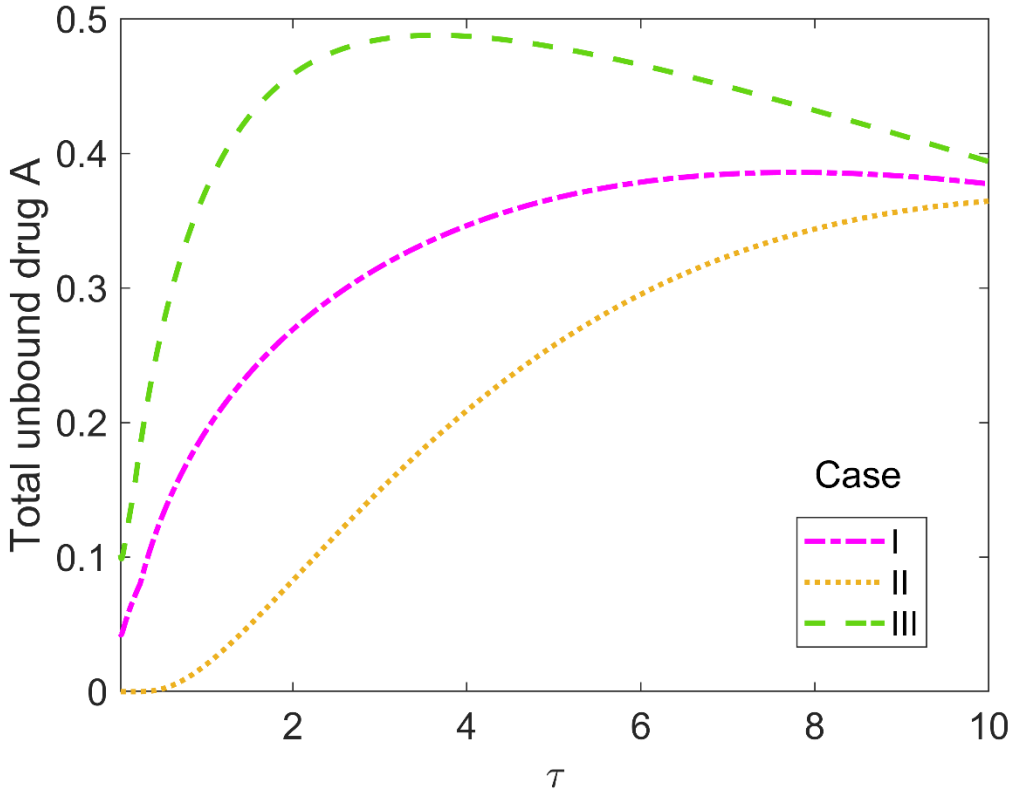

Figure 10 – Effect of initial drug distribution: Free sirolimus concentration as functions of time for three Cases I, II and III illustrated in Figure 1(b).

(REVISED) Table 1. Values of various problem parameters based on past work [6,9,16, 24-28]. A and B refer to sirolimus and paclitaxel, respectively. 1 and 2 refer to the stent coating and artery, respectively.

Symbol	Definition	Value	Unit	Reference
x_1	Thickness of stent coating	10	μm	[6]
$x_2 - x_1$	Thickness of artery	500	μm	[6]
c_{in}	Initial concentration of drugs A and B in layer 1	211	$mol \cdot m^{-3}$	[16]+
D_1^A	Diffusion coefficient of drug A in layer 1	1.2×10^{-16}	$m^2 \cdot s^{-1}$	[6]
D_1^B	Diffusion coefficient of drug B in layer 1	1.2×10^{-16}	$m^2 \cdot s^{-1}$	[6]
D_2^A	Diffusion coefficient of drug A in layer 2	7×10^{-12}	$m^2 \cdot s^{-1}$	[24]
D_2^B	Diffusion coefficient of drug B in layer 2	2×10^{-12}	$m^2 \cdot s^{-1}$	[24]
$\mu_1^{A,s}$	Forward specific reaction coefficient for drug A in layer 1	0	$m^3 \cdot s^{-1} \cdot mol^{-1}$	*
$\mu_1^{B,s}$	Forward specific reaction coefficient for drug B in layer 1	0	$m^3 \cdot s^{-1} \cdot mol^{-1}$	*
$\sigma_1^{A,s}$	Reverse specific reaction coefficient for drug A in layer 1	0	s^{-1}	*
$\sigma_1^{B,s}$	Reverse specific reaction coefficient for drug B in layer 1	0	s^{-1}	*
$\mu_2^{A,s}$	Forward specific reaction coefficient for drug A in layer 2	800	$m^3 \cdot s^{-1} \cdot mol^{-1}$	[25,26]
$\mu_2^{B,s}$	Forward specific reaction coefficient for drug B in layer 2	3.6×10^{-3}	$m^3 \cdot s^{-1} \cdot mol^{-1}$	[25,26]
$\sigma_2^{A,s}$	Reverse specific reaction coefficient for drug A in layer 2	1.6×10^{-4}	s^{-1}	[6,25]

$\sigma_2^{B,s}$	Reverse specific reaction coefficient for drug B in layer 2	9.1×10^{-2}	s^{-1}	[6,25]
$\mu_1^{A,ns}$	Forward non-specific reaction coefficient for drug A in layer 1	0	$m^3\cdot s^{-1}\cdot mol^{-1}$	*
$\mu_1^{B,ns}$	Forward non-specific reaction coefficient for drug B in layer 1	0	$m^3\cdot s^{-1}\cdot mol^{-1}$	*
$\sigma_1^{A,ns}$	Reverse non-specific reaction coefficient for drug A in layer 1	0	s^{-1}	*
$\sigma_1^{B,ns}$	Reverse non-specific reaction coefficient for drug B in layer 1	0	s^{-1}	*
$\mu_2^{A,ns}$	Forward non-specific reaction coefficient for drug A in layer 2	2	$m^3\cdot s^{-1}\cdot mol^{-1}$	[27,28]
$\mu_2^{B,ns}$	Forward non-specific reaction coefficient for drug B in layer 2	0.17	$m^3\cdot s^{-1}\cdot mol^{-1}$	[27,28]
$\sigma_2^{A,ns}$	Reverse non-specific reaction coefficient for drug A in layer 2	5.2×10^{-3}	s^{-1}	[6,27]
$\sigma_2^{B,ns}$	Reverse non-specific reaction coefficient for drug B in layer 2	5.27×10^{-4}	s^{-1}	[6,27]
$B_1^{A,s}$	Concentration of specific binding sites for drug A in layer 1	0	$mol\cdot m^{-3}$	*
$B_1^{B,s}$	Concentration of specific binding sites for drug B in layer 1	0	$mol\cdot m^{-3}$	*
$B_2^{A,s}$	Concentration of specific binding sites for drug A in layer 2	3.3×10^{-3}	$mol\cdot m^{-3}$	[9,25]
$B_2^{B,s}$	Concentration of specific binding sites for drug B in layer 2	1×10^{-2}	$mol\cdot m^{-3}$	[9,25]
B_1^{ns}	Concentration of non-specific binding sites in layer 1	0	$mol\cdot m^{-3}$	*
$B_2^{A,ns}$	Concentration of non-specific binding sites in layer 2 (Drug A)	0.363	$mol\cdot m^{-3}$	[9,25,28]

$B_2^{B,ns}$	Concentration of non-specific binding sites in layer 2 (Drug B)	0.117	$mol \cdot m^{-3}$	[9,25,28]

[+] This value is based on specifications of the XIENCE V stent.

* No binding is assumed to occur in the polymer layer.